Chromatin-associated lncRNA Malat1 regulates Th17 effector program and promotes intestinal inflammation

Shengyun Ma[1†], Bing Zhou[2,3†], Nicholas Chen[1], Claire Luo[1], Yuxin Li[1], Parth R. Patel[1], Anna Zheng[1], Shefali A. Patel[4], Yajing Hao[1], John T. Chang[4,5], Xiang-Dong Fu[1], Wendy Jia Men Huang[1]*

[1] Department of Cellular and Molecular Medicine, University of California San Diego, La Jolla, CA, USA
[2] State Key Laboratory of Stem Cell and Reproductive Biology, Institute of Zoology Chinese Academy of Sciences, Beijing, China
[3] Beijing Institute for Stem Cell and Regenerative Medicine, Beijing, China
[4] Department of Medicine, University of California San Diego, La Jolla, CA, USA
[5] Department of Medicine, Veterans Affairs San Diego Healthcare System, San Diego, CA, USA
[†] These authors contributed equally
* Correspondence: wendyjmhuang@health.ucsd.edu

Abstract

Interleukin IL-17 cytokines are central regulators of mucosal homeostasis and disease. In response to tissue injury, IL-17A promotes epithelial barrier functions and restricts local inflammation. In the resolution phase of colonic inflammation, adaptive Th17 cells are the major source of IL-17A, however, the cell-specific temporal control mechanism(s) underlying the delayed Th17 response remain elusive. Here, we discover a surprising role of the lncRNA Malat1 as a key barrier to achieving a robust and protective Th17 response. Genetic ablation of Malat1 potentiates IL-17A production in Th17 cells and improves disease outcomes in mouse models of colitis. Mechanistically, Malat1 represses *Il17a* transcription by restricting its bivalent super-enhancer activities. Thus, Malat1 is down-regulated during the resolution phase of inflammation, allowing Th17 to overtake early Tγδ17 as the major source of colonic IL-17A. Targeted depletion of Malat1 in T helper cell using anti-sense nucleotides show therapeutic potential in colitis model.

One Sentence Summary: Malat1 regulates super-enhancer transcriptional activities in Th17 cells.

INTRODUCTION

Inflammatory bowel disease (IBD) is a group of idiopathic inflammatory conditions in the digestive tract associated with the breakdown of epithelial barrier, microbial dysbiosis, immune hyperactivation, and abnormal tissue repair functions (*1*). The global prevalence of IBD is a major healthcare burden (*2*). Growing evidence suggests that IBD is likely initiated by a combination of genetic mutations and environmental factors giving rise to a "leaky" gut where microbes can breach the impaired epithelial barrier (*3, 4*). In response to these challenges, T cells in IBD patients are activated to secrete several immune modulatory cytokines, including interleukin 17 factors IL-17A and IL-17F (*5, 6*). These two cytokines are encoded in tandem on an evolutionarily conserved locus. Genetic polymorphisms of this locus have been associated with IBD susceptibility (*6, 7*).

Recent studies reported both physiological and pathological functions of IL-17 cytokines in different contexts. In multiple sclerosis, psoriasis, and cancers, IL-17 cytokines serve primary pro-inflammatory roles (*8-11*). In the intestine, however, IL-17 cytokines have been reported to have both pro- and anti-inflammatory properties. IL-17A enhances barrier function by stimulating intestinal epithelial cell proliferation and tight junction protein expression (*12-14*) and restricts local inflammation by recruiting myeloid suppressor cells (*15*). Neutralization of IL-17A or its receptor worsen intestine inflammation in IBD patients (*16, 17*). The protective role of IL-17A in the intestine is evolutionarily conserved and observed across multiple mouse models of colitis, including the $CD4^+$ T cell transfer (*12, 18*), the multidrug resistance-1a-ablated (Abcb1a(-/-))(*19*), and the dextran sulfate sodium (DSS)-induced models (*12, 20-22*). The role of IL-17F in intestinal inflammation is more complex. While Zhou et al reports reduced Treg accumulation and microbial dysbiosis in the $Il17f^{S65L/S65L}$ mice, previously used to model chronic oral candidiasis in human, resulted in worse DSS induced colitis outcome (*23*), Tang et al found increased Treg proportion and protection against DSS colitis in $Il17f^{-/-}$ mice (*11*). Adding to their functional complexity, IL-17 cytokines are secreted by multiple intestinal T cell subsets in a temporally regulated fashion. And how different subsets are regulated and contribute to IBD remain to be poorly defined. In the DSS model, Tγδ17 cells are the primary IL-17A-secreting population at the onset of disease. In the disease resolution phase, however, Th17 cells surpassed Tγδ17 cells as the main source of local IL-17A (*12, 15*). Little is unknown about the cell-specific mechanism(s) responsible for the delay in colonic Th17 responses and whether this temporal switch can be exploited for therapeutic intervention.

At the chromatin level, transcription of *Il17a* and its neighboring *Il17f* is controlled by a bivalent super-enhancer (SE) in Th17 cells (*24-27*). Bivalent SEs are large clusters of enhancers enriched with both active H3K27 acetylation (H3K27ac) and repressive tri-methylation (H3K27me3) marks, the latter of which results from methyltransferase activity of the Polycomb Repressive Complex 2 (PRC2) (*28, 29*). The bivalent chromatin state is thought to assure silencing of developmentally regulated genes while keeping them poised for activation during cell differentiation (*30, 31*). In Th17 cells, multiple transcription factors, including signal transducer and activator of transcription 3 (STAT3), RAR-related orphan receptor gamma (RORγt), SMAD Family Member 2 (SMAD2), and Tripartite motif containing 28 (TRIM28), have been implicated in promoting the expression of *Il17a* and *Il17f* (*24, 32-34*), but negative regulator(s) involved in establishing and maintaining the *Il17a-Il17f* bivalent SE has remained elusive.

Increasing evidence indicates that chromatin-associated long non-coding RNAs (lncRNAs) function as critical modulators of gene transcription (*35, 36*). Malat1 is the most abundantly expressed lncRNA in mammalian genomes and is ubiquitously expressed in all cell and tissue types, including T cells (*37, 38*). Surprisingly, mouse genetic studies show that this lncRNA is

dispensable for organ development, cell viability, fertility, and lifespan (*39-41*). Subcellularly, Malat1 are often found on the chromatin of actively transcribed genes, suggesting its vital role in organizing transcriptional hubs in the nucleus (*42, 43*). Additionally, this lncRNA has also been reported to partner with components of the PRC2 complex to promote histone H3K27 hypermethylation (*44-48*). However, it remains controversial in regulatory involvement of Matal1 in IBD, as MALAT1 expression is reported to be down-regulated in Crohn's disease patients (*49*), but up-regulated in ulcerative colitis cohorts (*50*). A recent study utilized the *Malat1*$^{LacZpA/LacZpA\ (RIKEN)}$ knockout mouse line to investigate the function of this lncRNA in the intestine and its contribution to intestinal diseases. However, the interpretation of the reported findings is questionable as *Malat1* in this model is only partially ablated and results are further confounded by the reduced expression of a *Malat1* nearby gene *Neat1* (*40*), another abundant lncRNA previously reported to be involved in intestine inflammation (*51*).

Here, we uncover a surprising role of Malat1 in repressing IL-17 cytokine production in Th17 cells using a well-characterized Malat1 knockout (*Malat1*$^{-/-}$) mouse line in which the Malat1 transcript is completely ablated without detectable effect on Neat1 expression (*41*). During the resolution phase of colitis, Malat1 is down-regulated, licensing Th17 to surpass Tγδ17 as the major IL-17A producer. Malat1 knockout mice equipped with elevated IL-17A production capacity in their Th17 cells undergo more rapid inflammation resolution when challenged with DSS-induced colitis. In a T cell-elicited colitis model, we further demonstrate that transiently depleting Malat1 in T helper cells provide disease protection.

RESULTS

Malat1 negatively correlates with *Il17a* expression in Th17 cells during DSS induced colitis

Previous studies suggest that IL-17A expression in Th17 cells is upregulated during the resolution phase of DSS-induced colitis (*15*). We reasoned that the molecular player(s) involved in temporally regulating this Th17 response is likely dynamically regulated. To identify putative regulators of Th17, we performed single cell transcriptomic analysis on colonic CD4^{+} T cells from wildtype mice before and after 2% DSS challenge in drinking water (Figure 1A). We found two *Il17a*-expressing populations, cluster C3 and C4 (Figure 1A-B). C3 cells responded to DSS by upregulating *Il17a*. In C4 cells, an intermediate population with both Th1 and Th17 gene signatures, *Il17a* expression was not sensitive to DSS (Figure 1C). Therefore, we focused on candidate genes whose expression pattern either positively or negatively correlated with *Il17a* levels in C3 cells as candidate regulators of Th17. Interestingly, Malat1 was the most abundantly expressed gene that showed a negative correlation with *Il17a* expression in C3 cells (Figure 1C-E). No additional correlations were found between *Il17a* and other detectable lncRNAs in these cells (Figure 1F). These results implied Malat1 might as a negative regulator of *Il17a* inTh17 cells.

To test whether Malat1 may be involved in regulating IL-17A expression in colonic Th17 cells and/or contribute to colitis pathogenesis, Malat1$^{-/-}$ and Malat1$^{+/+}$ (referred to as CTL from now) experimental pairs (*41*) were generated from heterozygous crosses (Figure S1A). Under steady state, Malat1$^{-/-}$ and CTL littermates had similar body weight (Figure S1B). T cell developments in the CTL and Malat1$^{-/-}$ thymus were comparable (Figure S1C-D). Steady state spleens from CTL and Malat1$^{-/-}$ mice harbored similar proportions of mature helper and cytotoxic T cells (Figure S2E). Also, we did not detect any difference in the percentage of splenic Treg (CD4^{+}CD25^{+}) or the ratio of naïve (CD62L^{+}CD44^{-}) versus activated (CD62L^{-}CD44^{+}) T helper subsets (Figure S2F-G). These data showed Malat1 was dispensable for thymic T cell development and mature T cells circulation in the periphery.

When challenged with DSS, Malat1$^{-/-}$ mice experienced less weight loss on day 8-10 compared to CTL littermates (Figure 2A). Colonic tissues from Malat1$^{-/-}$ mice displayed significantly less muscle thickening and submucosal inflammation (Figure 2B-C). These data revealed that Malat1 is a positive regulator of intestine inflammation *in vivo*. Next, we evaluated whether Malat1 regulates the expression of various immune modulatory cytokines previously implicated in colitis pathogenesis, including IL-17F and IFNγ with known pathogenic roles (*1, 11*) and IL-17A and IL-10 with protective roles in intestinal inflammation (*8, 12, 18*). At the RNA level, transcripts encoding IL-17A were elevated in total colonic lamina propria (cLP) cell lysates from DSS-challenged Malat1$^{-/-}$ mice (Figure 2D). Transcripts encoding IL-17F, and IFNγ were also elevated in the Malat1$^{-/-}$ cLP, but their absolute levels were magnitudes lower than those encoding IL-17A (Figure 2D). Notably, these changes in cytokine transcript levels were not due to alterations in the proportion of different T cell subsets (Figure 2E and S2A). At the protein level, in the DSS challenged Malat1$^{-/-}$ colon, IL-17A production was enhanced in Th17 cells, but not in Tr17 and Tγδ17 cells (Figure 2F-G and S2B). In contrast, steady state Malat1$^{-/-}$ mice did not displayed altered IL-17A expression in their colonic Th17 cells (Figure S2C), suggesting that Malat1 negatively regulates Th17 function only under settings of inflammation. We did not observe protein level change to IFNγ and IL-10 in CTL and Malat1$^{-/-}$ cLP T cells (Figure 2F and S2D). These results suggested that Malat1 selectively regulated IL-17A expression in Th17 cells during colitis.

We next checked whether the rapid colitis resolution observed in Malat1$^{-/-}$ mice is due to the absence of Malat1 in T cells in a model of T cell-mediated colitis. Naïve CD4^{+} T cells were isolated from CTL and Malat1$^{-/-}$ littermates and transferred to RAG1$^{-/-}$ recipients. RAG1$^{-/-}$ mice transplanted with Malat1$^{-/-}$ CD4^{+} T cells experienced less weight loss compared to those receiving CTL cells (Figure 2H). These data demonstrated that Malat1 in T cells is necessary to drive disease pathogenesis in colitis.

Malat1 regulates Th17 function in a cell autonomous manner

To further characterize the T cell intrinsic role of Malat1, we isolated naïve T cells from CTL and Malat1$^{-/-}$ mice and differentiated these cells toward different T helper lineages, including Th1, Th2, Th17 and Treg *in vitro* (Figure 3A). We found that Malat1 was dispensable for *in vitro* differentiation of naïve T cells toward Treg, Th1, and Th2 lineages (Figure S3A-D). When naïve cells were activated and polarized toward Th17 cells in the presence of IL-6 and TGFβ, a condition known to generate the non-pathogenic Th17 lineage (*52, 53*), we found that Malat1 ablation augmented IL-17A and IL-17F production in this lineage (Figure 3B), similar to our *in vivo* observations and consistent with results from a recent study using a transient knockdown approach (*54*). Importantly, such augmented cytokine levels observed in Malat1$^{-/-}$ Th17 cells were not due to altered expression of RORγt, the master transcription factor for the genes encoding these two cytokines (Figure 3C-D). At the RNA level, we also confirmed significant elevation of *Il17a* and *Il17f* transcripts in cultured Malat1$^{-/-}$ Th17 cells (Figure 3E), suggesting that Malat1 likely regulates these two genes transcriptionally and/or post-transcriptionally. In the presence of IL-6 in combination with IL-23 and/or IL-1b, polarizing conditions known to generate pathogenic Th17 cells (*52*), we did not detect any impact of Malat1 ablation on IL-17A and IL-17F production (Figure 3B). These findings established a selective role of Malat1 in repressing IL-17 cytokine production in Th17 cells downstream of TGFβ signaling.

Malat1-dependent regulation of gene expression in Th17 cells

Next, we asked whether Malat1 regulated the expression of other genes beyond *Il17a* and *Il17f* in Th17 cells polarized in the presence of IL-6 and TGFβ. RNA-seq analysis confirmed an increase of *Il17a* and *Il17f* transcripts in cultured Malat1$^{-/-}$ Th17 cells (Figure S4A-B) and identified additional Malat1-regulated genes encoding molecules involved in Th17 cell differentiation (*Pp3ca*), cell migration (*Arhgap5*, *Itgb1*), senescence (*Zfp36l1*, *Zfp36l2*), Hippo signaling (*Bmpr2*, *Ajuba*), and metabolism (*Dgat1*, *Aldh6a1*) (Figure S4C). Surprisingly, majority of Malat1-dependent genes reside outside of the Malat1 resident chromosome 19 (Figure S4D), suggesting that Malat1 exert greater regulatory functions on distal chromatins in Th17 cells. qRT-PCR analysis on independent cultures from additional pairs of CTL and Malat1$^{-/-}$ littermates confirmed several additional Malat1-regulated genes (Figure S4E), extending the regulatory role of Malat1 in cultured Th17 cells beyond cytokine production.

Malat1 is enriched on specific sites at the *Il17a-Il17f* super-enhancer

Given the preferential nuclear localization and enrichment on active chromatins of Malat1 in other cell-types (*41, 55*), we asked whether Malat1 also preferentially localized to the nucleus and/or occupied specific sites in Th17 cells. Single molecule RNA FISH assay revealed that majority of the Malat1 transcripts localized to the nucleus in both naïve and cultured Th17 cells (Figure 4A), similar to other cell types. Interestingly, a subset of Malat1 RNAs colocalized with the *Il17f* transcription hubs (indicated by triangles in Figure 4A). Therefore, we hypothesized that Malat1 might be recruited to the chromatin at or near the vicinity of the *Il17a-Il17f* locus to regulate local transcription.

To unbiasedly characterize the chromatin occupancy of Malat1 in Th17 cells, we took advantage of the GRID-seq approach recently developed to capture RNA-DNA interactions in the native nuclear 3D space (*56*). From two independent replicates of wildtype Th17 cells, we identified a total of 7,039 enriched Malat1-chromatin interactions (peaks), mostly on autosomes (Figure S5A). Unlike previous reports (*42, 57*), we detected the majority of Malat1 peaks (54.5%) were on gene promoters in comparison to 35.2% and 10.3% on gene bodies and intergenic regions respectively (Figure S5B-C). Regarding the open and active chromatin regions characterized by ATAC-seq and H3K27ac ChIP-seq, Malat1 preferred to occupy on the active regulatory elements, with 91.9% and 75.3% on active promoters and active intergenic regions respectively. Interestingly, almost one quarter of Malat1 binding on the inactive chromatin of intergenic regions implied some repressive roles of Malat1 on the epigenetic regulation, in line with previous discoveries that Malat1 partners with PRC2 complex to promote histone H3K27 hypermethylation (*44-48*). These results extend the reported role of Malal1 in organizing active gene hubs (*42, 43, 57*) to bipotential involvement in both gene activation and repression on distal chromatins.

A Malat1 region necessary for repressing IL-17 cytokine expressions in Th17 cells

In naïve T cells, ATAC-seq and GRID-seq results revealed the *Il17a-Il17f* locus displayed a closed chromatin configuration with little detectable Malat1 binding (Figure S6A-B). In Th17 cells, Malat1 occupied two open elements within the previously defined conserved non-coding site CNS3 and CNS4 (*58*) (Figure 4B and S6A). Intriguingly, five regions on the Malat1 transcript made close contact with the *Il17a-Il17f* chromatin (Figure 4B and S6A-B, referred as region A to E). Three of the five regions (B, C, and D) also made frequent contacts with other Malat1 targets (Figure 4C). These results imply that both shared and/or gene-specific mechanisms may underly

Malat1 regulation of Th17 targets and regions A and E may serve unique and/or gene-specific roles on *Il17a-Il17f*.

To explore the possibility that specific Malat1 region(s) is required for its regulatory role on Th17 targets, we attempted to use the CRISPR technology to introduce indel mutations on different regions of Malat1. For this purpose, we transduced activated $CD4^+$ T cells from Cas9 transgenic mice with retroviruses carrying region-specific sgRNA expression constructs. After confirming Cas9-sgRNA induced indel mutations by sequencing, we assessed whether specific sgRNA(s) can alter the expression of IL-17A and IL-17F. Interestingly, we found that two independent sgRNAs (sgA.1 and sgA.2) targeting region A (chr19: 5801450-5801521, GRCm38/mm10), but not sgRNAs targeting the other 4 regions (B-E) on Malat1, significantly augmented IL-17A and IL-17F at the mRNA and protein levels (Figure 4D-G), suggesting that region A on Malat1 is necessary for its ability to repress cytokine production in Th17 cells. Point mutations and insertions were the most frequently observed sgRNA induced indel mutations on region A (Figure 4E). Importantly, targeting of region A did not alter the overall Malat1 RNA abundance (Figure 4G), indicating that the impact on IL-17A and IL-17F was likely due to altered Malat1 RNA structure and/or function. Furthermore, we found that region A on Malat1 was dispensable for regulating other direct target genes, *Syncrip, Dgat1* and *Ddx3x* (Figure S6C-D). Together, these results implied that region A directed the gene-specific functions of Malat1, including repressing cytokine expression, in Th17 cells.

Malat1 contributes to the recruitment of PRC2 to the *Il17a-Il17f* bivalent super-enhancer

In Th17 cells, the *Il17a* gene body together with CNS2-CNS6 (*58*) form a vast open chromatin region with characteristics of a bivalent super-enhancer, decorated by both active and repressive marks including H3K27ac and H3K27me3 (*58, 59*) (Figure 5A-B). In other cell types, H3K27me3 deposition is mediated by PRC2 (*60, 61*) and recent studies using crosslinking immunoprecipitation sequencing (CLIP) assays reveal Malat1 binding to components of PRC2, including EZH2 and SUZ12 (*47, 62, 63*) (Figure 5C). On the *Il17a-Il17f* super-enhancer, SUZ12 signals (*59*) were most prominent around CNS3 and CNS4, where Malat1 was also enriched (Figure 5B). Therefore, we tested whether Malat1 is involved in recruitment of PRC2 and/or H3K27me3 deposition on the *Il17a-Il17f* bivalent SE to modulate the transcriptional output of the locus. ChIP-qPCR analysis of CTL and $Malat1^{-/-}$ Th17 cells indeed revealed that Malat1 ablation selectively and significantly diminished SUZ12 binding and H3K27me3 at the Malat1-occupying region CNS4. On nearby CNSs (CNS3 and CNS7), we also observed a modest, but not yet significant, reduction of Suz12 and H3K27me3 signals in $Malat1^{-/-}$ Th17 cells (Figure 5D, upper panels). This suggests the regulatory effect of Malat1 on this bivalent SE is likely spatially constrained. By contrast, no change was observed in other regions of the *Il17a-Il17f* SE, and H3K27 acetylation between CTL and $Malat1^{-/-}$ Th17 cells were comparable (Figure 5D, bottom panels). Together, these results strongly suggested a role of Malat1 in the recruitment of PRC2 to maintain the SE bivalency of the *Il17a-Il17f* locus (modeled in Figure 5E).

ASO targeting of Malat1 in T helper cells ameliorates colitis

To assess the potential of targeting Malat1 in T cells for ameliorating colitis, we designed an anti-sense nucleotide (ASO) that complementarily binds within region A (Figure 6A). *In vitro* cultured Th17 cells treated with this Malat1-specific ASO displayed higher RNA and protein expression of IL-17A and IL-17F compared to cells treated with CTL ASO (Figure 6B-C). In the T cell transfer colitis model, $RAG1^{-/-}$ mice receiving Malat1-specific ASO-treated $CD4^+$ T cells were protected

from weight loss (Figure 6D-E). Colonic lamina propria mononuclear cells from Malat1-specific ASO-treated recipients showed significantly lowered Malat1 abundance (Figure 6F), suggesting this transient strategy was effective in maintaining Malat1 depletion for more than 40 days *in vivo*. Importantly, Malat1-specific ASO-treated Th17 cells recovered from spleen displayed significant increase in IL-17A production potential, a similar but more modest effect was found in the cLP Th17 cells (Figure 6G-H). We also observed elevated IL-17F levels in Malat1-specific ASO-treated Th17 cells in the colon and spleen. Notably, IL-17F$^+$ Th17 cells were found in much lower proportion than IL-17A$^+$ Th17 cells in the transfer colitis model, similar to our observation in the DSS model (Figure 2D), suggesting a more dominant role of the Malat1-IL-17A axis *in vivo*. Together, these proof-of-concept experiments suggested that ASO targeting region A of Malat1 might be further explored as a therapeutic strategy against T cell-mediated intestinal inflammation.

DISCUSSION

IL-17A is a cytokine important in mucosal barrier maintenance with protective roles during intestinal inflammation (*12-14, 19, 20, 22, 64*). In the DSS-induced model of colitis, Tγδ17 cells are the primary source of early IL-17A production. As the disease progresses, the protective role of Tγδ17 cells is taken over by the gradually increased IL-17A-expressing Th17 cells emerging as the major source of IL-17A for tissue repair (*12, 15*). Although both Tγδ17 and Th17 cells are thought to be pre-programed to express IL-17A, mechanism(s) restricting early Th17 cell responses and how their effector function gets turned on later during colitis has long been elusive in the field. We now identified the lncRNA Malat1 as a key regulator of IL-17A expression in Th17 cells downstream of TGFβ, which is dramatically induced after epithlial injury and peak at resolution phase (*12*).

It is well known that IL-6 and TGFβ drive Th17 differentiation and promote cytokine production. Interestingly, results from this study reveal a surprising role of TGFβ in enabling the Malat1-dependent repressive machinery to fine-tune Th17 cytokine production quantitatively and temporally during colitis. It will be important for future studies to determine whether components of the TGFβ signaling machinery, including the SMAD family of transcription factors, may be involved in the proper positioning of Malat1 on the Th17 chromatin and/or promoting specific Malat1-protein complex assembly, including the Malat1-PRC2 module to exert a repressive role on the *Il17a-Il17f* locus. Although Tγδ17 cells also require signals from TGFβ for their proper thymic differentiation, it is unclear how these cells can escape from TGFβ-Malat1 regulation in the inflamed colon. One possibility maybe Tγδ17 cells do not express or express at low levels specific factors that Malat1 rely on, including those downstream of the TGFβ signaling cascade.

In the Th17 nucleus, our mechanistic studies demonstrate that Malat1 RNAs transcribed on chromosome 19 can translocate to the distal *Il17a-Il17f* SE on chromosome 1 to regulate the chromatin lanscape and gene expression. Knocking out *Malat1* and/or mutating a 5' region of Malat1 RNA result in *Il17a-Il17f* SE hyperactivation, thereby elevating cytokine production in Th17 cells. This provides a new paradigm for a lncRNA to function as the central player in maintaining SE bivalency to prevent Th17 hyperactivation. It will be interesting for future studies to explore whether changes in the *Il17a-Il17f* enhancer landscape in other IL-17 cytokine expressing immune cell subsets, such as Tr17, Tγδ17, NK17 and MAIT17 cells, would allow for and/or disable Malat1 regulation.

In cultured Th17 cells, Malat1 exerts regulation on both *Il17a* and *Il17f* (Figure 2B). IL-17A and IL-17F can form homodimers and IL-17A/IL-17F heterodimers (*65*). Recent studies suggest a complex role of IL-17F in intestinal inflammation. Zhou et al reported reduced Treg

accumulation and microbial dysbiosis in the Il17f$^{S65L/S65L}$ mice, previously used to model chronic oral candidiasis in human, resulted in worse DSS induced colitis outcome (*23*), whereas Tang et al found increased Treg proportion and protection against DSS colitis in Il17f$^{-/-}$ mice (*11*). In this report, we show that IL-17F^{+} Th17 cells were found in much lower proportion than IL-17A^{+} Th17 cells on day 10 of DSS induced colitis and day 43 of T cell mediated colitis (Figure 1E, 2D and 6G-H). In the absence of Malat1, we did not observe significant changes to the colonic Treg proportions at these time points. Therefore, we suspect that the regulatory function of Malat1 on IL-17A production likely outweight its role on IL-17F at the time points that we investigate in these models (Figure 1G). To assess the possible biological role of the Malat1-IL-17F axis, future studies will need to utilize a more relevant disease time point and/or employ the well-characterized IL-17F-dependent disease models, such as the *Il1rn*$^{-/-}$ autoimmune arthritis and *Citrobacter rodentium* challenges (*66*).

We speculate that if future therapeutic strategy can be developed to target anti-sense nucleotides specifically to T helper cell for Malat1 depletion, it may help boost IL-17A production in Th17 cells, thereby accelerating inflammation resolution to protect against colitis. This strategy would mimick in essence an endogenous mechansim that downregulated Malat1 in colonic Th17 cells during the resolution phase of inflammation (day 10 in the DSS model). Interestingly, down-regulation of Malat1 has also been observed in the TNBS-induce colitis model as well as in Cohn's diseases patients (*49*). Whether common or model/disease-specific pathways are implicated in dampening Malat1 expression in these different situations and the degree to which quantitative changes in Malat1 levels would alter bivalency at the *Il17a-Il17f* SE, IL-17A expression, and disease outcomes merit further dissection in future studies.

In summary, our results shed new light on the chromatin localization and immunological function of Malat1 in Th17 cells, highlighting the previously unrecognized role of this lncRNA in restricting the mucosal protective function of Th17 cells and providing new opportunities for developing therapeutic intervention strategies to treat IBD.

MATERIALS AND METHODS

Study Design

Intestinal homeostasis and inflammation are tightly regulated by interleukin IL-17 cytokines. In response to intestine injury, IL-17A promotes epithelial barrier functions and restricts local inflammation. In the resolution phase of colonic inflammation, adaptive Th17 cells are the major source of IL-17A. This study investigates how this pathway is temporally restricted by the long non-coding RNA (lncRNA) Malat1 in Th17 cell-specific manner. To this end, we performed single-cell transcriptomic analysis in the mouse model of dextran sulfate (DSS) induced colitis to identify lncRNAs displaying temporally dynamic expression patterns in colonic lamina propria T cells. We elucidated the *in vivo* function of Malat1 in DSS-induced and T-cell transfer models of colitis using the Malat1 knockout mice (Malat1$^{-/-}$). We characterized Malat1-dependent gene programs by transcriptomic profiling and mapped the chromatin localization of Malat1 genome-wide using the global RNA interactions with DNA by deep sequencing (GRID-seq) approach in naïve and Th17 cells. Antisense nucleotide (ASO) was used to assess therapeutic potential of this pathway.

Mice

C57BL/6 wild-type (Stock No: 000664), Cas9 (Stock No: 026179) and RAG1$^{-/-}$ (Stock No: 002216) were obtained from the Jackson Laboratory. Malat1$^{-/-}$ mice were obtained from Dr. David Spector's laboratory and have been previously described (*41*). Heterozygous mice were bred to yield 6-8 weeks old CTL (Malat1$^{+/+}$ or Malat1$^{+/-}$) and Malat1$^{-/-}$ littermates. Gender matched cohoused littermates at least eight weeks old were used. All animal studies were approved and followed the Institutional Animal Care and Use Guidelines of the University of California San Diego.

DSS-induced and T cell transfer colitis

Mice were provided 2% (w/v) DSS (160110; MP, Bio-medicals) in their drinking water for 7 days, followed by 3 days of access to regular drinking water. Mice weights were monitored daily, and tissues were harvested on day 10. Pathology scoring of distal colons from steady state and DSS-challenged mice was performed blind following previously published guidelines (*67*), including parameters for muscle thickening and submucosal inflammation. For adoptive transfer model of colitis, 0.5 million naive CD4^{+} T cells isolated from mouse splenocytes using the Naive CD4^{+} T Cell Isolation Kit (Miltenyi) were injected intraperitoneally into RAG1$^{-/-}$ recipients. Mice weights were measured twice a week for 21 days.

Anti-sense nucleotide (ASO) experiments were designed following best practice guidelines (*68*). 2′-deoxy-2′-fluoro-D-arabinonucleic acid (2′-FANA) containing CTL ASOs targeting a Trypanosoma gene (GCCGTTTACGTCGTCACAGA) or Malat1 (TTCTTTGCCTATCTTGAATGC) were purchased from AUM BIOTECH and their purities were confirmed by MALDI. ASOs were incubated with activated CD4^{+} T cell *in vitro* for 48hrs according to manufacturer instructions (AUM BIOTECH). ASO treated cells (2x10^{6}) were then introduced to RAG1$^{-/-}$ mice by intraperitoneal injection. Mice weights were measured every 6 days, tissues were harvested on day 43 for flow cytometry analysis.

Flow Cytometry

To probe for cytokine production potential, cells were stimulated with 5 ng/mL Phorbol 12-myristate 13-acetate (PMA, Millipore Sigma) and 500 ng/mL ionomycin (Millipore Sigma) in the presence of GolgiStop (BD Bioscience) for 5 hours at 37 ˚C. Antibodies for cell surface molecules were incubated with intact live cells. Following fixation and permeabilization (eBioscience), antibodies for intracellular transcription factors and cytokines were added. Antibodies are listed in Table S2.

***In vitro* T Cell Culture**

Mouse naive T cells were purified from spleens and lymph nodes of 8-12 weeks old mice using the Naive CD4^{+} T Cell Isolation Kit according to the manufacturer's instructions (Miltenyi). Cells were cultured in Iscove's Modified Dulbecco's Medium (IMDM, Sigma Aldrich) supplemented with 10% heat-inactivated FBS (Peak Serum), 50 U penicillin-streptomycin (Life Technologies), 2 mM glutamine (Life Technologies), and 50 μM β-mercaptoethanol (Sigma Aldrich). For cell polarization, naive cells were seeded in 24-well or 96-well plates pre-coated with rabbit anti-hamster IgG and cultured for 72 hours in the presence of 0.25 μg/mL anti-CD3ε (eBioscience), 1 μg/mL anti-CD28 (eBioscience) and different cytokines for different cell differentiation. IL-2 (15 U/mL) and IL-12β (10 μg/mL) for Th1; IL-2 (15 U/mL) and IL-4 (10 μg/mL) for Th2; IL-2 (15

U/mL) and TGFβ (5 μg/mL) for Treg; IL-6 (20 ng/mL) and/or TGFβ (0.1 ng/mL), IL-1β (20 μg/mL), IL-23 (100 μg/mL) for Th17. All the cytokines were obtained from R&D Systems.

Retrovirus Transduction in T cells

Malat1 specific sgRNAs were designed by CHOPCHOP (*69*). sgRNA sequences are listed in Table S1. pSIN retroviral constructs carrying expression cassettes for sgRNA along with a surface protein CD90.1 (Thy1.1) were generated as described previously (*70*). PlatE cells were used to generate retrovirus as described (*71*). Virus transduction in $Cas9^+$ $CD4^+$ T cells were performed 24 hours after T cell activation (0.25 μg/mL anti-CD3ε, 1 μg/mL anti-CD28) by centrifugation at 2000 rpm for 90 min at 32 ºC. Live and $Thy1.1^+$ transduced cells cultured in Th17 polarizing conditions were analyzed by flow cytometry at 72 hrs.

scRNA-seq and analysis

Colonic lamina propria cells from DSS or non-DSS treated mice were collected and enriched for $CD4^+$ T cells using the mouse $CD4^+$ T cell Isolation Kit (Miltenyi). Enriched $CD4^+$ cells (~10,000 per mouse) were prepared for single cell libraries using the Chromium Single Cell 3' Reagent Kit (10xGenomics). The pooled libraries of each sample (20,000 reads/cell) were sequenced on one lane of NovaSeq S4 following manufacturer's recommendations. Cellranger v3.1.0 was used to filter, align, and count reads mapped to the mouse reference genome (mm10-3.0.0). The Unique Molecular Identifiers (UMI) count matrix obtained was used for downstream analysis using Seurat (v4.0.1). The cells with mitochondrial counts >5%, as well as outlier cells in the top and bottom 0.2% of the total gene number detected index were excluded. After filtering, randomly selected 10,000 cells per sample were chosen for downstream analysis. Initial cell clusters identified by Seurat with low expression of *Cd4* or *Cd3e* (mean log-transformed gene expression < 1) were removed, resulting in 10,308 total cells from eight samples. These cells were scaled and normalized using log-transformation, and the top 6,000 genes were selected for principal component analysis. The dimensions determined from PCA were used for clustering and UMAP visualizations.

Average gene expression in CPM (counts per million) in each cell clusters were used in calculation of fold changes between DSS and non-DSS treated samples. To avoid unconfident noise of gene expression occasionally observed in cell clusters, significant changes of gene expression in each cell cluster were identified here by a cutoff of 1.3-fold changes with averaged expression of each comparing pairs no less than 1 CPM in the DSS and non-DSS treated samples.

RNA-seq

Ribosome-depleted RNAs were used to prepare sequencing libraries. 100 bp paired-end sequencing was performed on an Illumina HiSeq4000 by the Institute of Genomic Medicine at the University of California San Diego. Each sample yielded approximately 30-40 million reads. Paired-end reads were aligned to the mouse mm10 genome with the STAR aligner version 2.6.1a (*72*) using the parameters: "--outFilterMultimapNmax 20 --alignSJoverhangMin 8 --alignSJDBoverhangMin 1 --outFilterMismatchNmax 999 --outFilterMismatchNoverReadLmax 0.04 --alignIntronMin 20 --alignIntronMax 1000000 --alignMatesGapMax 1000000". Uniquely mapped reads overlapping with exons were counted using featureCounts (*73*) for each gene in the GENCODE.vM19 annotation. Differential expression analysis was performed using DESeq2 (v1.18.1 package) (*74*), including a covariate in the design matrix to account for differences in

harvest batch/time points. Regularized logarithm (rlog) transformation of the read counts of each gene was carried out using DESeq2. Pathway analysis was performed on differentially expressed protein coding genes with minimal counts of 10, $\log_2$ fold change cutoffs of ≥ 0.4 or ≤-0.4, and p-values <0.05 using GeneCodis4.0.

GRID-seq

GRID-seq of naïve and cultured Th17 cells were performed as described (*56, 75*). Briefly, two independent biological replicates (5-10 $\times 10^6$) were crosslinked with disuccinimidyl glutarate (DSG) and formaldehyde. DNA in isolated nuclei were digested with AluI. A biotinylated bivalent linker was ligated to chromatin-associated RNA (with the ssRNA stretch on the linker) and nearby fragmented genomic DNA and captured by streptavidin microbeads for library construction. Single-end sequencing was performed on HiSeq400 (Illumina, 200 million reads/sample).

Raw sequencing reads were evaluated by FastQC (*76*). Reads below 85bp were filtered out and those above 90bp with high quality were trimmed by Cutadapt (*77*) as suggested according to previous report (*56, 75*). The GRID-seq linker position at each read and the paired reads originated from RNA or genomic DNA were identified by matefq in GridTools (*75*). Paired RNA and DNA reads were then mapped to the mouse genome (GRCm38/mm10) by BWA respectively. Uniquely paired reads were used to generate a set of RNA-DNA interaction matrix for downstream analyses in the GridTools pipeline. Read counts from the two repeats were summarized into two 1kb genomic bins. Chromatin enriched with Malat1 RNAs (GRID-seq peak call) were defined as 2kb regions with clustered Malat1 signals above the background signal expected from random interactions (> 5-fold changes). In total, 7,039 regions out of 30,321 bins were identified as enriched Malat1 peaks for further analysis. Interactions of Malat1 RNA with Th17 genomic DNA were plotted in circos by circlize (*76*).

ChIP-qPCR, ChIP-seq, and ATAC-seq

ChIP was performed on 5-10 million Th17 cells crosslinked with 1% formaldehyde. Chromatin was sonicated and immunoprecipitated using antibodies listed in Table S2 and captured on Dynabeads (ThermoFisher Scientific). Immunoprecipitated protein-DNA complexes were reverse cross-linked and chromatin DNA purified as described in (*78*). ChIP-qPCR primer sequences are listed in Table S1.

ATAC-seq libraries were generated as described in (*79*). ChIP-seq and ATAC-seq processing followed the ENCODE guideline with some modifications (*80*). Specifically, single-end raw reads were mapped to the mouse genome (GENCODE assembly mm10) by bowtie2 (Version 2.3.4.1) in the local mapping mode with parameter "--local", followed by PCR deduplication by SAMTools (Version 1.9) with the utility markedup (*81*). Mapped reads from each sample repeats were merged into a single BAM file by SAMTools, and peaks were called using MACS2 (Version 2.2.6) (*82*) in the narrow peak-calling mode with default parameters for ChIP-seq data or specific parameters of "callpeak --nomodel --extsize 100" for ATAC-seq data. Regions with peak-score below 30 were filtered out and the remaining reliable peak profiles were transformed into bigwig format and visualized on the Integrative Genomics Viewer (IGV Version 2.8.2) (*83*).

Super-enhancers were identified by normalized H3K27ac signals in genomic regions within a 12.5 Kb window outside of any known-gene promoters (TSS ± 2.5 Kb) based on the algorithm as

previously reported (*28, 84*). Briefly, any genomic regions calculated with overall H3K27ac coverage higher than the geometrically defined inflection point were considered putative super-enhancers and those below were consider putative typical enhancers.

cDNA Synthesis and qRT-PCR

Total RNA was extracted with the RNeasy kit (QIAGEN) and reverse transcribed using Superscript III (Life technology). Real time RT-PCR was performed using iTaq™ Universal SYBR® Green Supermix (Bio-Rad Laboratories). Gene expressions were normalized to *Gapdh* mRNA levels. qRT-PCR primers were designed using Primer-BLAST to span across splice junctions, resulting in PCR amplicons that span at least one intron. Primer sequences are listed in Table S1.

RNA FISH

RNA FISH was performed followed the protocol from BIOSERARCH TECHNOLOGIES. Briefly, cells were fixed with 3.7% formaldehyde and permeabilized with 70% ethanol, followed with hybridization with stellaris RNA FISH probes (Malat1-Cy3 and Il17f-Cy5). Nuclear DNA was visualized by 4′,6-diamidino-2-phenylindole (DAPI) and imaged with Leica SP8 confocal microscope.

Statistical Analysis

All values are presented as means ± SD. Significant differences were evaluated using GraphPad Prism 8 software. The student's t-test or paired t-test were used to determine significant differences between two groups. A two-tailed p-value of <0.05 was considered statistically significant in all experiments.

Supplementary Materials

Figs. S1 to S6.

Tables S1 to S3.

References and Notes

1. M. Friedrich, M. Pohin, F. Powrie, Cytokine Networks in the Pathophysiology of Inflammatory Bowel Disease. *Immunity* **50**, 992-1006 (2019).
2. G. B. D. I. B. D. Collaborators, The global, regional, and national burden of inflammatory bowel disease in 195 countries and territories, 1990-2017: a systematic analysis for the Global Burden of Disease Study 2017. *Lancet Gastroenterol Hepatol* **5**, 17-30 (2020).
3. Q. Mu, J. Kirby, C. M. Reilly, X. M. Luo, Leaky Gut As a Danger Signal for Autoimmune Diseases. *Front Immunol* **8**, 598 (2017).
4. M. A. Odenwald, J. R. Turner, The intestinal epithelial barrier: a therapeutic target? *Nat Rev Gastroenterol Hepatol* **14**, 9-21 (2017).
5. S. Fujino *et al.*, Increased expression of interleukin 17 in inflammatory bowel disease. *Gut* **52**, 65-70 (2003).
6. J. Seiderer *et al.*, Role of the novel Th17 cytokine IL-17F in inflammatory bowel disease (IBD): upregulated colonic IL-17F expression in active Crohn's disease and analysis of the IL17F p.His161Arg polymorphism in IBD. *Inflamm Bowel Dis* **14**, 437-445 (2008).

7. S. W. Kim *et al.*, Genetic polymorphisms of IL-23R and IL-17A and novel insights into their associations with inflammatory bowel disease. *Gut* **60**, 1527-1536 (2011).
8. M. J. McGeachy, D. J. Cua, S. L. Gaffen, The IL-17 Family of Cytokines in Health and Disease. *Immunity* **50**, 892-906 (2019).
9. S. Buonocore *et al.*, Innate lymphoid cells drive interleukin-23-dependent innate intestinal pathology. *Nature* **464**, 1371-1375 (2010).
10. A. Chaudhry *et al.*, CD4+ regulatory T cells control TH17 responses in a Stat3-dependent manner. *Science* **326**, 986-991 (2009).
11. C. Tang *et al.*, Suppression of IL-17F, but not of IL-17A, provides protection against colitis by inducing Treg cells through modification of the intestinal microbiota. *Nat Immunol* **19**, 755-765 (2018).
12. X. Song *et al.*, Growth Factor FGF2 Cooperates with Interleukin-17 to Repair Intestinal Epithelial Damage. *Immunity* **43**, 488-501 (2015).
13. T. Kinugasa, T. Sakaguchi, X. Gu, H. C. Reinecker, Claudins regulate the intestinal barrier in response to immune mediators. *Gastroenterology* **118**, 1001-1011 (2000).
14. J. S. Lee *et al.*, Interleukin-23-Independent IL-17 Production Regulates Intestinal Epithelial Permeability. *Immunity* **43**, 727-738 (2015).
15. X. Sun *et al.*, Innate gammadeltaT17 cells play a protective role in DSS-induced colitis via recruitment of Gr-1(+)CD11b(+) myeloid suppressor cells. *Oncoimmunology* **6**, e1313369 (2017).
16. W. Hueber *et al.*, Secukinumab, a human anti-IL-17A monoclonal antibody, for moderate to severe Crohn's disease: unexpected results of a randomised, double-blind placebo-controlled trial. *Gut* **61**, 1693-1700 (2012).
17. S. R. Targan *et al.*, A Randomized, Double-Blind, Placebo-Controlled Phase 2 Study of Brodalumab in Patients With Moderate-to-Severe Crohn's Disease. *Am J Gastroenterol* **111**, 1599-1607 (2016).
18. W. O'Connor, Jr. *et al.*, A protective function for interleukin 17A in T cell-mediated intestinal inflammation. *Nat Immunol* **10**, 603-609 (2009).
19. J. R. Maxwell *et al.*, Differential Roles for Interleukin-23 and Interleukin-17 in Intestinal Immunoregulation. *Immunity* **43**, 739-750 (2015).
20. X. O. Yang *et al.*, Regulation of inflammatory responses by IL-17F. *J Exp Med* **205**, 1063-1075 (2008).
21. R. Ito *et al.*, Involvement of IL-17A in the pathogenesis of DSS-induced colitis in mice. *Biochem Biophys Res Commun* **377**, 12-16 (2008).
22. A. Ogawa, A. Andoh, Y. Araki, T. Bamba, Y. Fujiyama, Neutralization of interleukin-17 aggravates dextran sulfate sodium-induced colitis in mice. *Clin Immunol* **110**, 55-62 (2004).
23. C. Zhou *et al.*, Divergent functions of IL-17-family cytokines in DSS colitis: Insights from a naturally-occurring human mutation in IL-17F. *Cytokine* **148**, 155715 (2021).
24. Y. Jiang *et al.*, Epigenetic activation during T helper 17 cell differentiation is mediated by Tripartite motif containing 28. *Nat Commun* **9**, 1424 (2018).
25. D. Pham *et al.*, Batf Pioneers the Reorganization of Chromatin in Developing Effector T Cells via Ets1-Dependent Recruitment of Ctcf. *Cell Rep* **29**, 1203-1220 e1207 (2019).
26. K. L. Cheung *et al.*, Distinct Roles of Brd2 and Brd4 in Potentiating the Transcriptional Program for Th17 Cell Differentiation. *Mol Cell* **65**, 1068-+ (2017).
27. S. Witte, A. Bradley, A. J. Enright, S. A. Muljo, High-density P300 enhancers control cell state transitions. *BMC Genomics* **16**, 903 (2015).
28. D. Hnisz *et al.*, Super-enhancers in the control of cell identity and disease. *Cell* **155**, 934-947 (2013).
29. A. Mantsoki, K. Parussel, A. Joshi, Identification and Characterisation of Putative Enhancer Elements in Mouse Embryonic Stem Cells. *Bioinform Biol Insights* **15**, 1177932220974623 (2021).
30. V. Azuara *et al.*, Chromatin signatures of pluripotent cell lines. *Nat Cell Biol* **8**, 532-538 (2006).
31. G. E. Zentner, P. J. Tesar, P. C. Scacheri, Epigenetic signatures distinguish multiple classes of enhancers with distinct cellular functions. *Genome Res* **21**, 1273-1283 (2011).
32. X. O. Yang *et al.*, STAT3 regulates cytokine-mediated generation of inflammatory helper T cells. *J Biol Chem* **282**, 9358-9363 (2007).
33. Ivanov, II *et al.*, The orphan nuclear receptor RORgammat directs the differentiation program of proinflammatory IL-17+ T helper cells. *Cell* **126**, 1121-1133 (2006).
34. N. Malhotra, E. Robertson, J. Kang, SMAD2 is essential for TGF beta-mediated Th17 cell generation. *J Biol Chem* **285**, 29044-29048 (2010).
35. X. Han *et al.*, Mouse knockout models reveal largely dispensable but context-dependent functions of lncRNAs during development. *J Mol Cell Biol* **10**, 175-178 (2018).

36. L. Statello, C. J. Guo, L. L. Chen, M. Huarte, Gene regulation by long non-coding RNAs and its biological functions. *Nat Rev Mol Cell Biol* **22**, 96-118 (2021).
37. G. Arun, D. Aggarwal, D. L. Spector, MALAT1 Long Non-Coding RNA: Functional Implications. *Noncoding RNA* **6**, (2020).
38. O. M. de Goede *et al.*, Population-scale tissue transcriptomics maps long non-coding RNAs to complex disease. *Cell*, (2021).
39. M. Eissmann *et al.*, Loss of the abundant nuclear non-coding RNA MALAT1 is compatible with life and development. *Rna Biol* **9**, 1076-1087 (2012).
40. S. Nakagawa *et al.*, Malat1 is not an essential component of nuclear speckles in mice. *Rna* **18**, 1487-1499 (2012).
41. B. Zhang *et al.*, The lncRNA Malat1 is dispensable for mouse development but its transcription plays a cis-regulatory role in the adult. *Cell Rep* **2**, 111-123 (2012).
42. J. A. West *et al.*, The long noncoding RNAs NEAT1 and MALAT1 bind active chromatin sites. *Mol Cell* **55**, 791-802 (2014).
43. S. A. Quinodoz *et al.*, Higher-Order Inter-chromosomal Hubs Shape 3D Genome Organization in the Nucleus. *Cell* **174**, 744-757 e724 (2018).
44. H. Hirata *et al.*, Long Noncoding RNA MALAT1 Promotes Aggressive Renal Cell Carcinoma through Ezh2 and Interacts with miR-205. *Cancer Res* **75**, 1322-1331 (2015).
45. X. Wang *et al.*, LncRNA MALAT1 promotes development of mantle cell lymphoma by associating with EZH2. *J Transl Med* **14**, 346 (2016).
46. D. Wang *et al.*, LncRNA MALAT1 enhances oncogenic activities of EZH2 in castration-resistant prostate cancer. *Oncotarget* **6**, 41045-41055 (2015).
47. N. H. El Said *et al.*, Malat-1-PRC2-EZH1 interaction supports adaptive oxidative stress dependent epigenome remodeling in skeletal myotubes. *Cell Death Dis* **12**, 850 (2021).
48. S. Guil *et al.*, Intronic RNAs mediate EZH2 regulation of epigenetic targets. *Nat Struct Mol Biol* **19**, 664-670 (2012).
49. Y. Li *et al.*, MALAT1 maintains the intestinal mucosal homeostasis in Crohn's disease via the miR-146b-5p-CLDN11/NUMB pathway. *J Crohns Colitis*, (2021).
50. M. Zhu, J. Xie, LncRNA MALAT1 Promotes Ulcerative Colitis by Upregulating lncRNA ANRIL. *Dig Dis Sci* **65**, 3191-3196 (2020).
51. R. Liu *et al.*, Inhibition of lncRNA NEAT1 suppresses the inflammatory response in IBD by modulating the intestinal epithelial barrier and by exosome-mediated polarization of macrophages. *Int J Mol Med* **42**, 2903-2913 (2018).
52. K. Ghoreschi *et al.*, Generation of pathogenic T(H)17 cells in the absence of TGF-beta signalling. *Nature* **467**, 967-971 (2010).
53. M. J. McGeachy *et al.*, TGF-beta and IL-6 drive the production of IL-17 and IL-10 by T cells and restrain T(H)-17 cell-mediated pathology. *Nat Immunol* **8**, 1390-1397 (2007).
54. F. Masoumi *et al.*, Malat1 long noncoding RNA regulates inflammation and leukocyte differentiation in experimental autoimmune encephalomyelitis. *J Neuroimmunol* **328**, 50-59 (2019).
55. J. N. Hutchinson *et al.*, A screen for nuclear transcripts identifies two linked noncoding RNAs associated with SC35 splicing domains. *BMC Genomics* **8**, 39 (2007).
56. X. Li *et al.*, GRID-seq reveals the global RNA-chromatin interactome. *Nat Biotechnol* **35**, 940-950 (2017).
57. J. M. Engreitz *et al.*, RNA-RNA interactions enable specific targeting of noncoding RNAs to nascent Pre-mRNAs and chromatin sites. *Cell* **159**, 188-199 (2014).
58. R. M. Thomas, H. Sai, A. D. Wells, Conserved intergenic elements and DNA methylation cooperate to regulate transcription at the il17 locus. *J Biol Chem* **287**, 25049-25059 (2012).
59. T. M. Escobar *et al.*, miR-155 activates cytokine gene expression in Th17 cells by regulating the DNA-binding protein Jarid2 to relieve polycomb-mediated repression. *Immunity* **40**, 865-879 (2014).
60. X. Shen *et al.*, EZH1 mediates methylation on histone H3 lysine 27 and complements EZH2 in maintaining stem cell identity and executing pluripotency. *Mol Cell* **32**, 491-502 (2008).
61. G. van Mierlo, G. J. C. Veenstra, M. Vermeulen, H. Marks, The Complexity of PRC2 Subcomplexes. *Trends Cell Biol* **29**, 660-671 (2019).
62. M. Rosenberg *et al.*, Motif-driven interactions between RNA and PRC2 are rheostats that regulate transcription elongation. *Nature Structural & Molecular Biology* **28**, (2021).
63. S. Kaneko, J. Son, S. S. Shen, D. Reinberg, R. Bonasio, PRC2 binds active promoters and contacts nascent RNAs in embryonic stem cells. *Nat Struct Mol Biol* **20**, 1258-1264 (2013).

64. K. M. Buckley *et al.*, IL17 factors are early regulators in the gut epithelium during inflammatory response to Vibrio in the sea urchin larva. *Elife* **6**, (2017).
65. J. F. Wright *et al.*, The human IL-17F/IL-17A heterodimeric cytokine signals through the IL-17RA/IL-17RC receptor complex. *J Immunol* **181**, 2799-2805 (2008).
66. H. Ishigame *et al.*, Differential roles of interleukin-17A and -17F in host defense against mucoepithelial bacterial infection and allergic responses. *Immunity* **30**, 108-119 (2009).
67. P. J. Koelink *et al.*, Development of Reliable, Valid and Responsive Scoring Systems for Endoscopy and Histology in Animal Models for Inflammatory Bowel Disease. *J Crohns Colitis* **12**, 794-803 (2018).
68. K. T. Gagnon, D. R. Corey, Guidelines for Experiments Using Antisense Oligonucleotides and Double-Stranded RNAs. *Nucleic Acid Ther* **29**, 116-122 (2019).
69. K. Labun *et al.*, CHOPCHOP v3: expanding the CRISPR web toolbox beyond genome editing. *Nucleic Acids Res* **47**, W171-W174 (2019).
70. F. A. Ran *et al.*, Genome engineering using the CRISPR-Cas9 system. *Nat Protoc* **8**, 2281-2308 (2013).
71. S. Morita, T. Kojima, T. Kitamura, Plat-E: an efficient and stable system for transient packaging of retroviruses. *Gene Ther* **7**, 1063-1066 (2000).
72. A. Dobin *et al.*, STAR: ultrafast universal RNA-seq aligner. *Bioinformatics* **29**, 15-21 (2013).
73. Y. Liao, G. K. Smyth, W. Shi, featureCounts: an efficient general purpose program for assigning sequence reads to genomic features. *Bioinformatics* **30**, 923-930 (2014).
74. M. I. Love, W. Huber, S. Anders, Moderated estimation of fold change and dispersion for RNA-seq data with DESeq2. *Genome Biol* **15**, 550 (2014).
75. B. Zhou *et al.*, GRID-seq for comprehensive analysis of global RNA-chromatin interactions. *Nat Protoc* **14**, 2036-2068 (2019).
76. Z. Gu, L. Gu, R. Eils, M. Schlesner, B. Brors, circlize Implements and enhances circular visualization in R. *Bioinformatics* **30**, 2811-2812 (2014).
77. M. Martin, Cutadapt removes adapter sequences from high-throughput sequencing reads. *2011* **17**, 3 (2011).
78. M. U. Kaikkonen *et al.*, Remodeling of the enhancer landscape during macrophage activation is coupled to enhancer transcription. *Mol Cell* **51**, 310-325 (2013).
79. J. D. Buenrostro, B. Wu, H. Y. Chang, W. J. Greenleaf, ATAC-seq: A Method for Assaying Chromatin Accessibility Genome-Wide. *Curr Protoc Mol Biol* **109**, 21 29 21-21 29 29 (2015).
80. S. G. Landt *et al.*, ChIP-seq guidelines and practices of the ENCODE and modENCODE consortia. *Genome Res* **22**, 1813-1831 (2012).
81. H. Li *et al.*, The Sequence Alignment/Map format and SAMtools. *Bioinformatics* **25**, 2078-2079 (2009).
82. Y. Zhang *et al.*, Model-based analysis of ChIP-Seq (MACS). *Genome Biol* **9**, R137 (2008).
83. H. Thorvaldsdottir, J. T. Robinson, J. P. Mesirov, Integrative Genomics Viewer (IGV): high-performance genomics data visualization and exploration. *Brief Bioinform* **14**, 178-192 (2013).
84. W. A. Whyte *et al.*, Master transcription factors and mediator establish super-enhancers at key cell identity genes. *Cell* **153**, 307-319 (2013).
85. M. Ciofani *et al.*, A validated regulatory network for Th17 cell specification. *Cell* **151**, 289-303 (2012).

Acknowledgments
We thank David Spector at Cold Spring Harbor Laboratory for sharing the Malat1$^{-/-}$ mice. We thank Johannes Zuber and Aichinger Martin at the Research Institute of Molecular Pathology (I.M.P.) for sharing the pSIN vector for generating retroviruses to introduce custom sgRNAs into T cells.

Funding:

Edward Mallinckrodt, Jr. Foundation (WJMH)
National Institutes of Health grant R01GM124494 (WJMH)
National Institutes of Health grant P01 AI132122, BX005106, and P30DK120515 (JTC)
National Institutes of Health grant HG004659, DK098808, S10 OD026929, P30 CA23100
Strategic Priority Research Program of the Chinese Academy of Sciences XDA16010113 (BZ)
National Key Research and Development Program of China 2019YFA0110002 and 2019YFA0801700 (BZ)

Author contributions:

Conceptualization: WJMH, SM, BZ
Methodology: SM, BZ, WJMH, XDF
Investigation: SM, BZ, NC, CL, YL, PRP, AZ
Visualization: SM, SP, NC, SAP, YH, WJMH
Funding acquisition: WJMH, JTC
Project administration: WJMH
Supervision: JTC, XDF, WJMH
Writing – original draft: SM, BZ, WJMH
Writing – review & editing: WJMH, SM, XDF, JTC

Competing interests: All authors declare no competing financial interests.

Figure 1. **Malat1 negatively correlates with *Il17a* expression in colonic Th17 cells from DSS challenged mice**

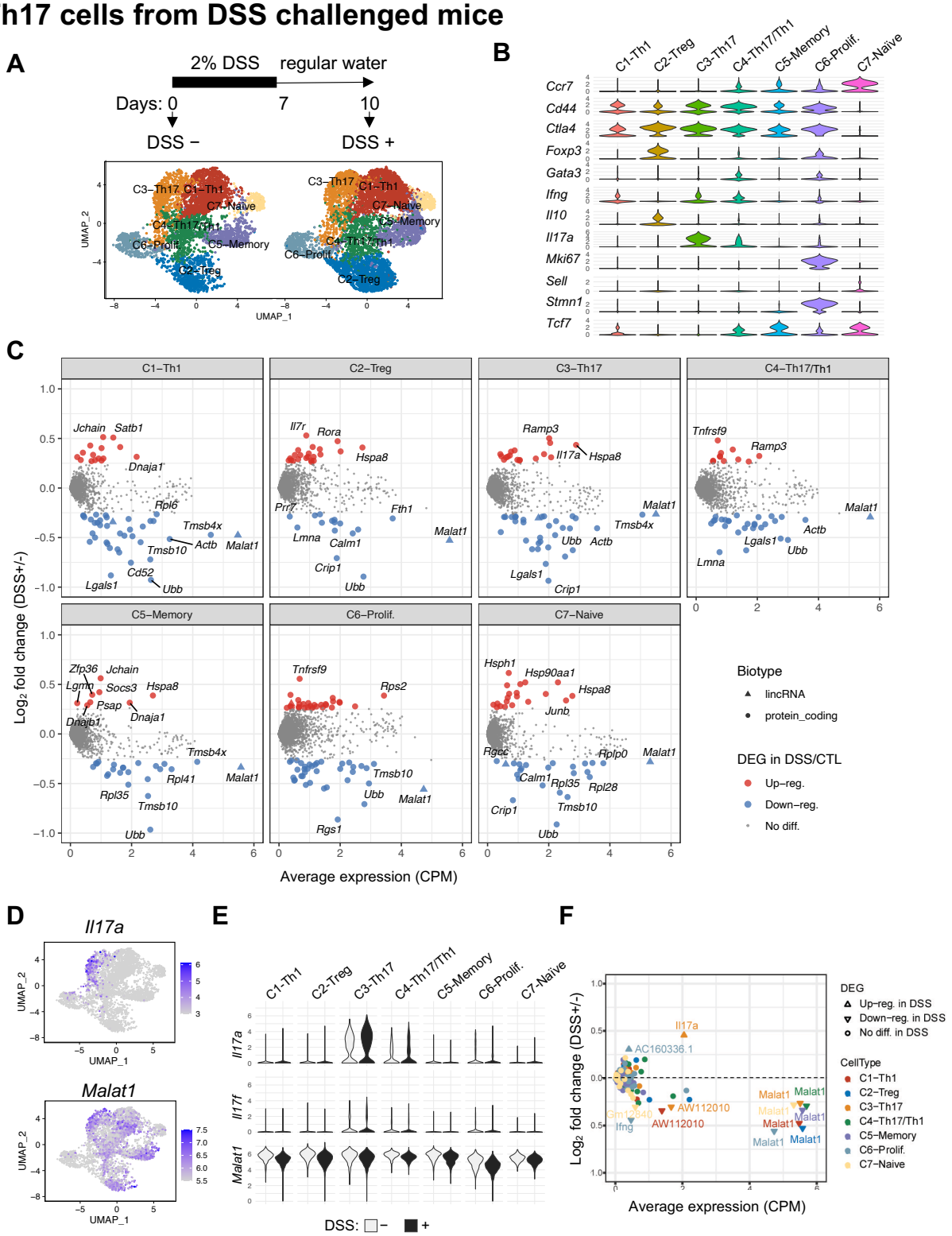

Figure 1. **Malat1 negatively correlates with *Il17a* expression in colonic Th17 cells from DSS-challenged mice**

A. UMAP plot of the seven clusters of $CD4^+$ T cells, including Th1 (cluster C1), Treg (C2), Th17 (C3), Th17-Th1 (C4), memory (C5), proliferating (C6) and naïve (C7) cells from colonic lamina propria of CTL (DSS -) and DSS treated mice (DSS +).
B. Expression of select cluster-specific genes in seven $CD4^+$ T cell clusters from A.
C. Expression of cluster specific cytokine genes and DSS regulated genes in each of the seven $CD4^+$ T cell clusters from mice treated with (+) or without (-) DSS.
D. UMAP plots of *Malat1* and *Il17a* expressions in cLP $CD4^+$ T cells.
E. Violin plot of *Il17a*, *Il17f*, and *Malat1* expressions in different T cell subsets from DSS challenged (+) or control (-) colons.
F. The MA plot shows the gene expression changes of 17 detected lncRNAs and 4 protein coding mRNAs (*Il17a* and *Ifng*) in each cell cluster described in A from control (-) and DSS treated (+) mice. LncRNAs or mRNAs labeled are those significantly up- or down-regulated in DSS treated mice.

Figure 2. **Malat1 in CD4⁺ T helper cells augments colonic inflammation**

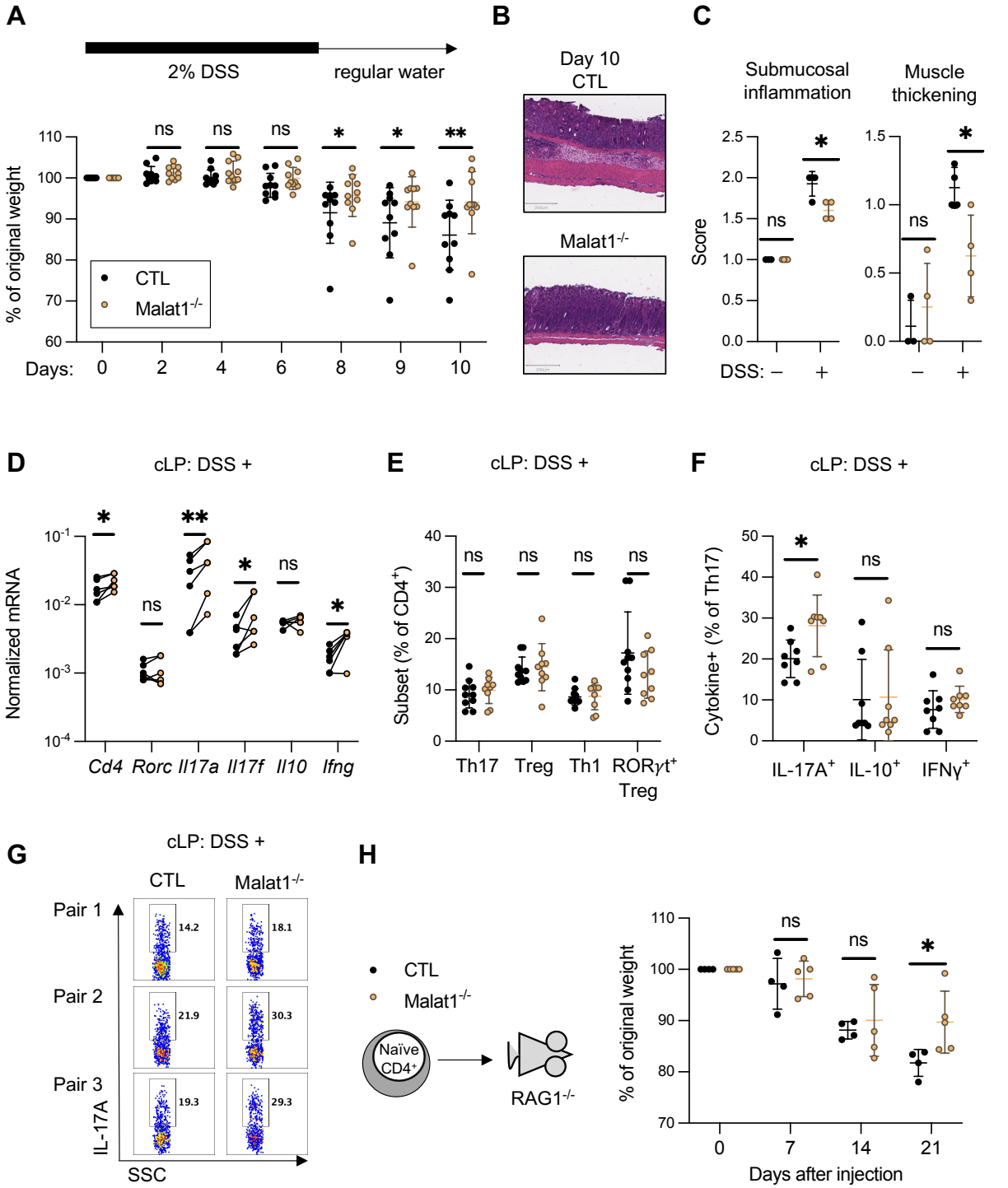

Figure 2. **Malat1 in CD4$^+$ T helper cells augments colonic inflammation**

A. Weight change of CTL (Malat1$^{+/+}$ or Malat1$^{+/-}$) (black, n=10) and Malat1$^{-/-}$ (red, n=9) cohoused littermates challenged with 2% DSS in drinking water for 7 days and regular water for an additional 3 days. Each dot represents result from one mouse. * p-value<0.05, ** p-value<0.01, ns: not significant (multiple t-test).
B. Representative H&E staining of colonic sections from CTL and Malat1$^{-/-}$ mice harvested on Day 10. Scale bar: 200mm.
C. Colonic submucosal inflammation and muscle thickening scores in CTL and Malat1$^{-/-}$ mice treated with or without DSS. DSS treated tissues were harvested on day 10. Each dot represents result from one mouse. * p-value<0.05, ns: not significant (t-test, n=4).
D. Normalized mRNA of the indicated genes relative to *Gapdh* in total colonic lamina propria mononuclear cells harvested from Malat1$^{-/-}$ and CTL mice on day 10 post initial DSS treatment as detected by qRT-PCR. Each dot represents result from one mouse. * p-value<0.05, ** p-value<0.01, ns: not significant (t-test, n=5).
E. Proportion of cLP Th17 (CD4$^+$ RORγt$^+$Foxp3$^-$), Treg (CD4$^+$ RORγt$^-$Foxp3$^+$), Th1 (CD4$^+$Tbet$^+$ RORγt$^-$), and RORγt$^+$ Treg (CD4$^+$ RORγt$^+$Foxp3$^+$) from CTL and Malat1$^{-/-}$ mice harvested on day 10 post DSS treatment. Each dot represents result from one mouse (t-test).
F. Proportion of cLP Th17 cells expressing the indicated cytokines from the of DSS treated CTL and Malat1$^{-/-}$ mice harvested on day 10. Each dot represents result from one mouse. * p-value<0.05, ns: not significant (t-test).
G. Representative flow cytometry analysis of IL-17A in cLP Th17 cells from 3 pairs of DSS treated CTL and Malat1$^{-/-}$ mice from G. SSC side scatter, an indicator of cell granularity.
H. Weight changes of RAG1$^{-/-}$ mice receiving CTL (n=4) or Malat1$^{-/-}$ (n=6) naive CD4$^+$ T cells. Each dot represents result from one RAG1$^{-/-}$ mouse. * p-value<0.05 (t-test).

Figure 3. **Malat1 negatively regulates cytokine production in cultured Th17**

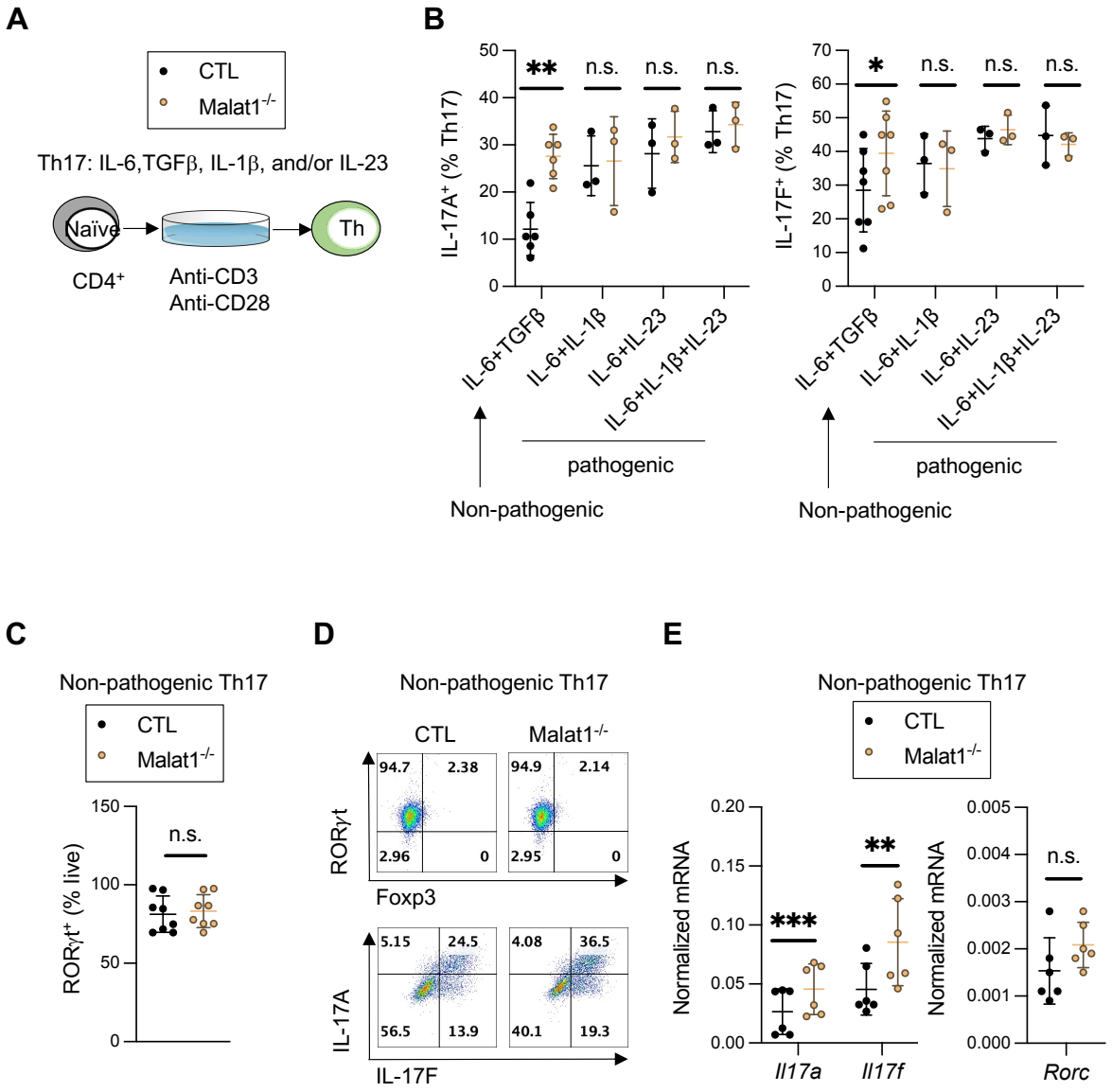

Figure 3. Malat1 negatively regulates cytokine production in cultured Th17 cells

A. Workflow for polarizing naïve $CD4^+$ T cell toward different Th17 subsets *in vitro*.
B. Summarized proportion of IL-17A and IL-17F in CTL and $Malat1^{-/-}$ $ROR\gamma t^+$ Th17 cells cultured with the indicated cytokines for 3 days. Each dot represents result from one independent culture. ** p-value<0.01, * p-value<0.05, n.s. not significant (paired t-test).
C. Summarized proportion of $ROR\gamma t^+$ Th17 cells from CTL and $Malat1^{-/-}$ littermates cultured in the presence of anti-CD3, anti-CD28, IL-6, and TGFβ for 3 days. Each dot represents result from one independent culture. n.s. not significant (paired t-test, n=8).
D. Representative flow cytometry analysis of RORγt, IL-17A, and IL-17F expression of CTL and $Malat1^{-/-}$ Th17 cells described in C.
E. Normalized mRNA of *Rorc*, *Il17a*, and *il17f* relative to *Gapdh* in cultured CTL and $Malat1^{-/-}$ Th17 cells from C as detected by qRT-PCR. Each dot represents result from one independent culture. ** p-value<0.01, *** p-value<0.001, n.s. not significant (paired t-test, n=5).

Figure 4. **A Malat1 RNA region implicated in *Il17a-Il17f* transcriptional repression**

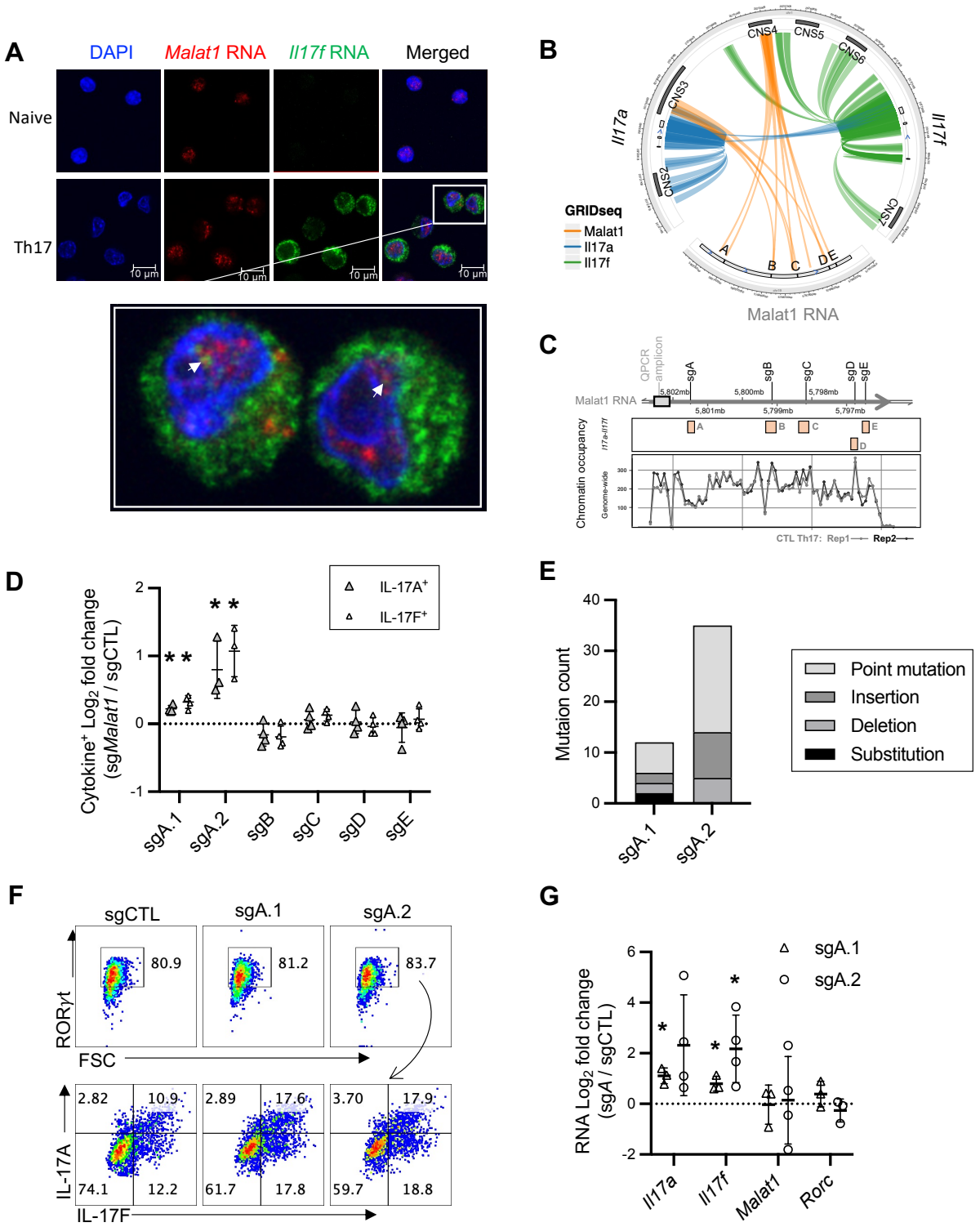

Figure 4. **A Malat1 RNA region implicated in *Il17a-Il17f* transcriptional repression**

A. Immunofluorescence in situ hybridization (RNA-FISH) detection of Malat1 RNA (red) and *Il17f* (green) mRNA in cultured CTL naïve and Th17 cells. DAPI (blue): nuclear DNA stain. White arrows: regions of *Malat1* and *Il17f* RNA co-localization in the Th17 nucleus. Scale bar: 5mm.
B. Circos plot showing the interactions between RNAs transcribed from *Il17a* (blue), *Il17f* (green), *Malat1* (orange) loci and chromatin DNA at the *Il17a-Il17f* locus in CTL Th17 cells captured by GRID-seq. Five regions on the Malat1 RNA found in close proximity to the *Il17a-Il17f* locus were designated as A-E.
C. Comparing Malat1 RNA regions enriched on Th17 chromatin genome-wide and those found in close proximity to *Il17a-Il17f* chromatin from 4B. Vertical black lines indicate positions of Malat1-specific small guide (sg) RNAs.
D. Summarized $\log_2$ fold change of flow cytometry analysis of IL-17A and IL-17F in $Cas9^+$ Th17 cells transduced with retroviral constructs expressing sgRNAs targeting each *Malat1* regions noted in A relative to those with CTL (empty vector). Each dot represents result from one independent culture. * p-value<0.05 (t-test).
E. SANGER sequencing results revealed diverse indel mutations generated by sgRNAs targeting region A.
F. Representative flow cytometry analysis of RORγt, IL-17A and IL-17F expression from B.
G. Summarized $\log_2$ fold change of relative RNA levels of the indicated genes in cultured $Cas9^+$ Th17 cells transduced with retroviral constructs expressing sgA relative to those with CTL vector. Each dot represents result from one independent culture. * p-value<0.05 (t-test).

Figure 5. **Malat1 recruits PRC2 to modulate *Il17a-Il17f* SE bivalency in Th17 cells**

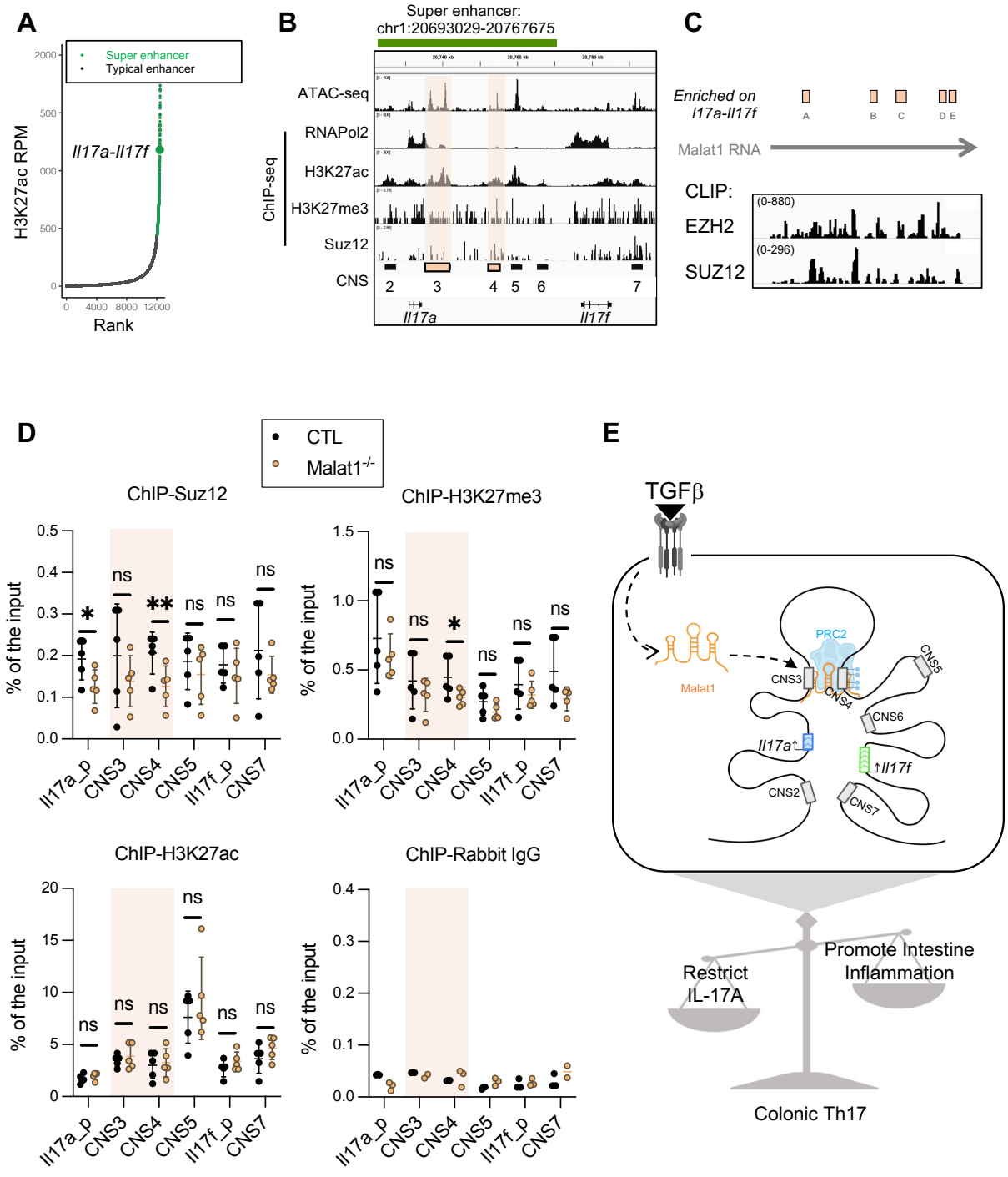

Figure 5. **Malat1 recruits PRC2 to modulate *Il17a-Il17f* SE bivalency in Th17 cells**

A. Th17 super-enhancers (green dots) and typical enhancers (black dots) were defined by regional H3K27ac signals (RPM) (see Methods for detail). Green big dot highlights the *Il17a-Il17f* locus.
B. IGV browser view of open chromatin signals as detected by ATAC-seq along with RNA Polymerase II (RNAPol2), H3K27ac, and the publicly available H3K27me3 and SUZ12 (GSE 47528) signals on the *Il17a-Il17f* locus in Th17 cells as detected by ChIP-seq.
C. IGV browser showing CLIP-seq signal of EZH2 (*63*) and SUZ12 (*62*) on murine Malat1 RNA.
D. ChIP-qRT analysis of H3K27me3, H3K27ac, Suz12, and Rabbit IgG (negative control) at the *Il17a-Il17f* locus in cultured Th17 cells from CTL and Malat1$^{-/-}$ mice. Each dot represents result from one independent culture. p, promoter. * p-value<0.05, n.s. not significant (paired t-test).
E. Model: Malat1 inhibits IL-17 cytokine production in Th17 cells by recruiting SUZ12 to down-regulating *Il17a-Il17f* super-enhancer activities. Genetic knockout of Malat1 or antisense oligonucleotide (ASO) treatments protect mice against T cell mediated colonic inflammation.

Figure 6. **Malat1-specific ASO regulates cytokine production in cultured and *in vivo* Th17 cells**

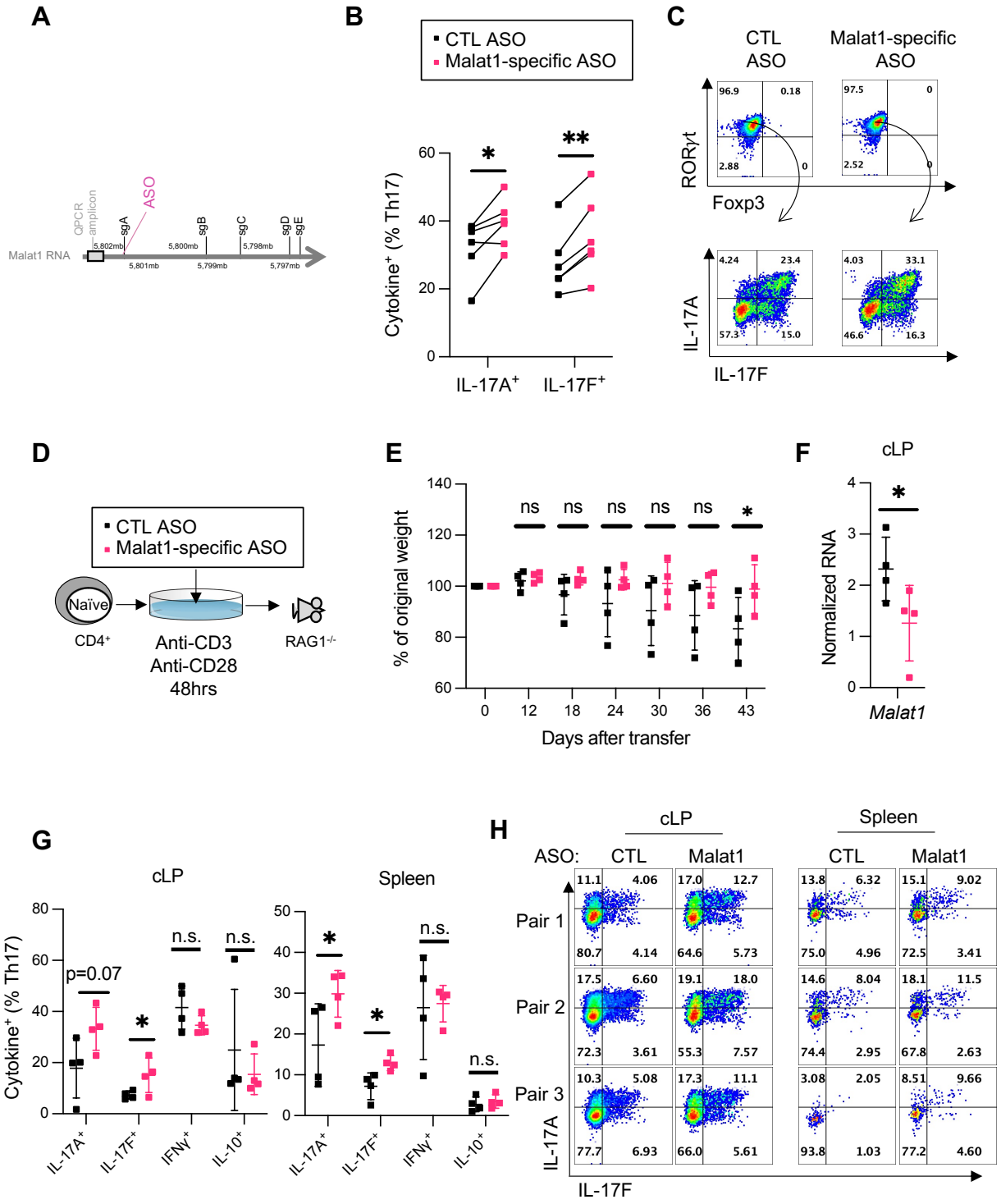

Figure 6. **Malat1-specific ASO regulates cytokine production in culture and *in vivo* Th17 cells**

A. Position of custom ASO targeting the Malat1 transcript.
B. Summarized flow cytometry analysis of IL-17A and IL-17F in cultured Th17 cells treated with CTL or Malat1-specific ASO. Each dot represents result from one independent culture. * p-value<0.05, ** p-value<0.01 (paired t-test, n=5).
C. Representative flow cytometry analysis of RORγt, Foxp3, IL-17A and IL-17F from B.
D. Workflow for treating $CD4^+$ T cell with CTL or Malat1-specific ASO and introducing the treated cells to $RAG1^{-/-}$ recipients by i.p. injection.
E. Weight changes of $RAG1^{-/-}$ mice receiving CTL (n=4) or Malat1-specific ASO treated $CD4^+$ T cells (n=4). Each dot represents result from one mouse. * p-value<0.05, n.s. not significant (t-test).
F. Normalized RNA level of *Malat1* in cLP cells from $RAG1^{-/-}$ mice shown in E. Each dot represents result from one mouse. * p-value<0.05 (t-test, n=4).
G. Summarized flow cytometry analysis of indicated cytokines in Th17 cells ($CD4^+ROR\gamma t^+Foxp3^-$) of cLP and spleen from $RAG1^{-/-}$ mice shown in E. Each dot represents result from one mouse. * p-value<0.05, n.s. not significant (t-test).
H. Representative flow cytometry analysis of IL-17A and IL-17F in colonic Th17 cells described in G.

Supplementary Figure

Figure S1. **Normal thymic T cell development and splenic T cell populations in Malat1$^{-/-}$ mice**

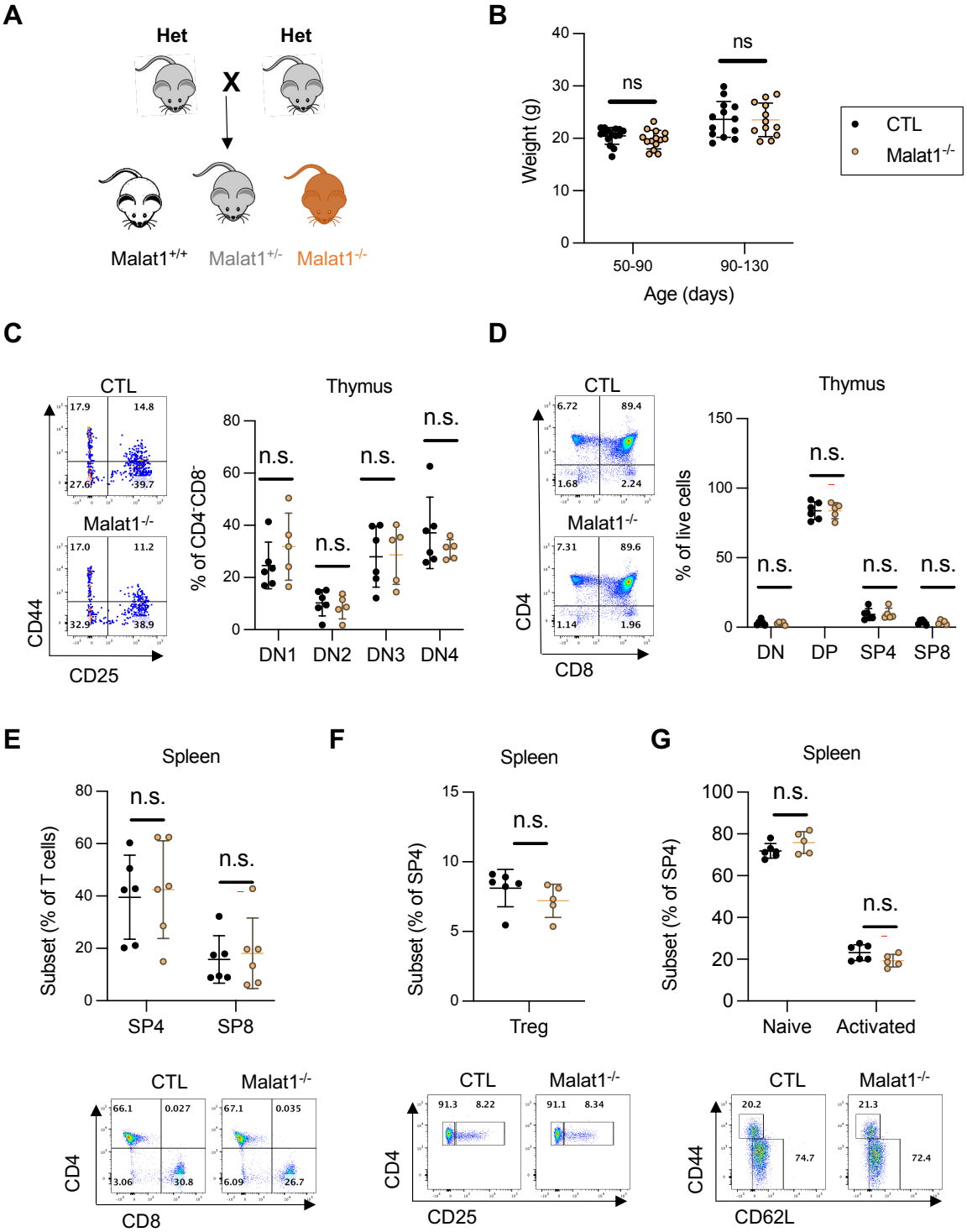

Figure S1. **Normal thymic T cell development and splenic T cell populations in Malat1$^{-/-}$ mice.**

A. Heterozygous crosses to generate Malat1$^{+/+}$, Malat1$^{+/-}$, and Malat1$^{-/-}$ gender matched and cohoused littermates for experiments described in this study.
B. Weight of CTL (Malat1$^{+/+}$ or Malat1$^{+/-}$) (n=30) and Malat1$^{-/-}$ (n=28) mice assessed at the indicated ages. Each dot represents result from one mouse. ns: no significant (t-test).
C. Representative flow cytometry analysis (left) and summarized percentage (right) of thymic DN subsets (DN1: CD44^{-}CD25^{-}, DN2: CD44^{+}CD25^{-}, DN3: CD44^{+}CD25^{+}, and DN4: CD44^{-}CD25^{+}) from CTL and Malat1$^{-/-}$ mice. n.s. not significant (paired t-test, n=5).
D. Representative flow cytometry analysis (left) and summarized percentage (right) of thymic developing T cells (DN: CD4^{-}CD8^{-}, SP4: CD4^{+}CD8^{-}, SP8: CD4^{-}CD8^{+}, and DP: CD4^{+}CD8^{+}) from CTL and Malat1$^{-/-}$ mice. n.s. not significant (paired t-test, n=6).
E. Summarized percentage (top) and representative flow cytometry results (bottom) of CD4 and CD8 expression in total spleenocytes from CTL and Malat1$^{-/-}$ mice. n.s. not significant (paired t-test, n=6).
F. Summarized percentage (top) and representative flow cytometry results (bottom) of Tregs (CD25^{+}) among spleenic CD4^{+} cells from CTL and Malat1$^{-/-}$ mice. n.s. not significant (paired t-test, n=6).
G. Summarized percentage (top) and representative flow cytometry results (bottom) of naïve (CD44^{-}CD62L^{+}) and activated (CD44^{+}CD62L^{-}) CD4^{+} T helper cells from CTL and Malat1$^{-/-}$ spleen. n.s. not significant (paired t-test, n=5).

Figure S2. **Cytokine expressions in different colonic T cell populations in Malat1$^{-/-}$ mice under DSS challenge and steady state.**

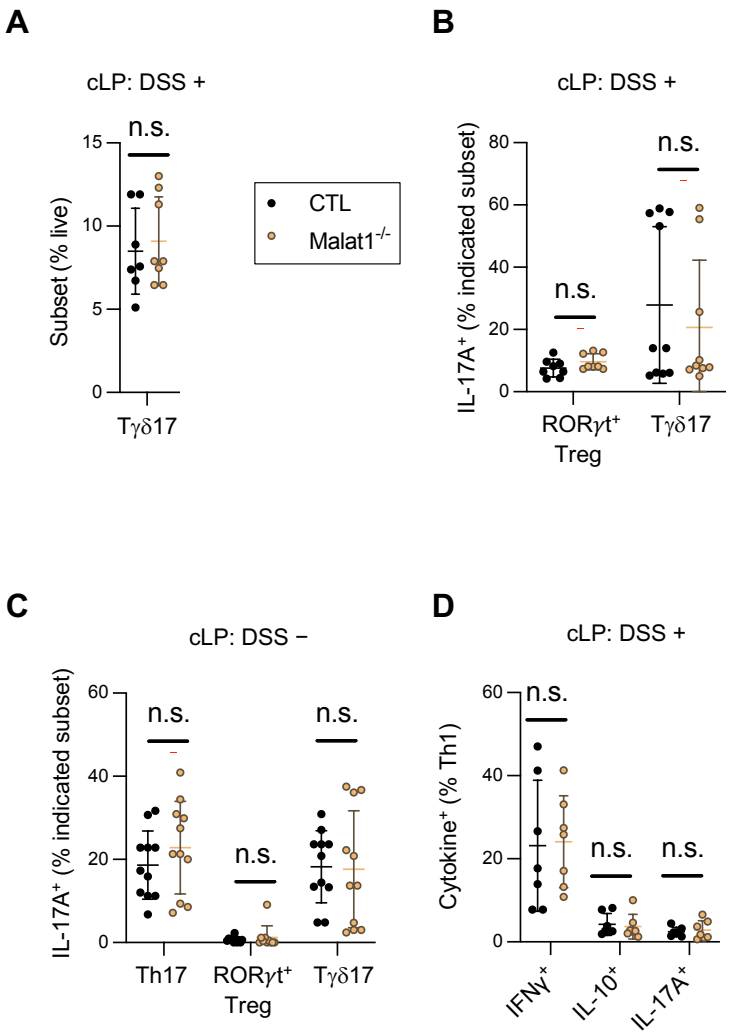

Figure S2. **Cytokine expressions in different colonic T cell populations in Malat1$^{-/-}$ mice under DSS challenge and steady state**

A. Proportion of cLP Tγδ17 (TCRγδ^{+}RORγt^{+}) cells from CTL and Malat1$^{-/-}$ mice harvested on day 10 post DSS treatment. n.s. not significant (t-test).
B. Proportion of cLP RORγt^{+} Treg and Tγδ17 cells expressing IL-17A from CTL and Malat1$^{-/-}$ mice harvested on day 10 post DSS treatment. n.s. not significant (t-test, n=9).
C. Proportion of cLP Th17, RORγt^{+} Treg, and Tγδ17 cells expressing IL-17A and IL-17F from steady state CTL and Malat1$^{-/-}$ mice. n.s. not significant (t-test, n=11).
D. Proportion of cLP Th1 cells expressing the indicated cytokines from DSS-challenged CTL and Malat1$^{-/-}$ mice. n.s. not significant. (t-test, n=7).

Figure S3. **Malat1 does not regulate Th1, Th2, and Treg generation and function *in vitro***

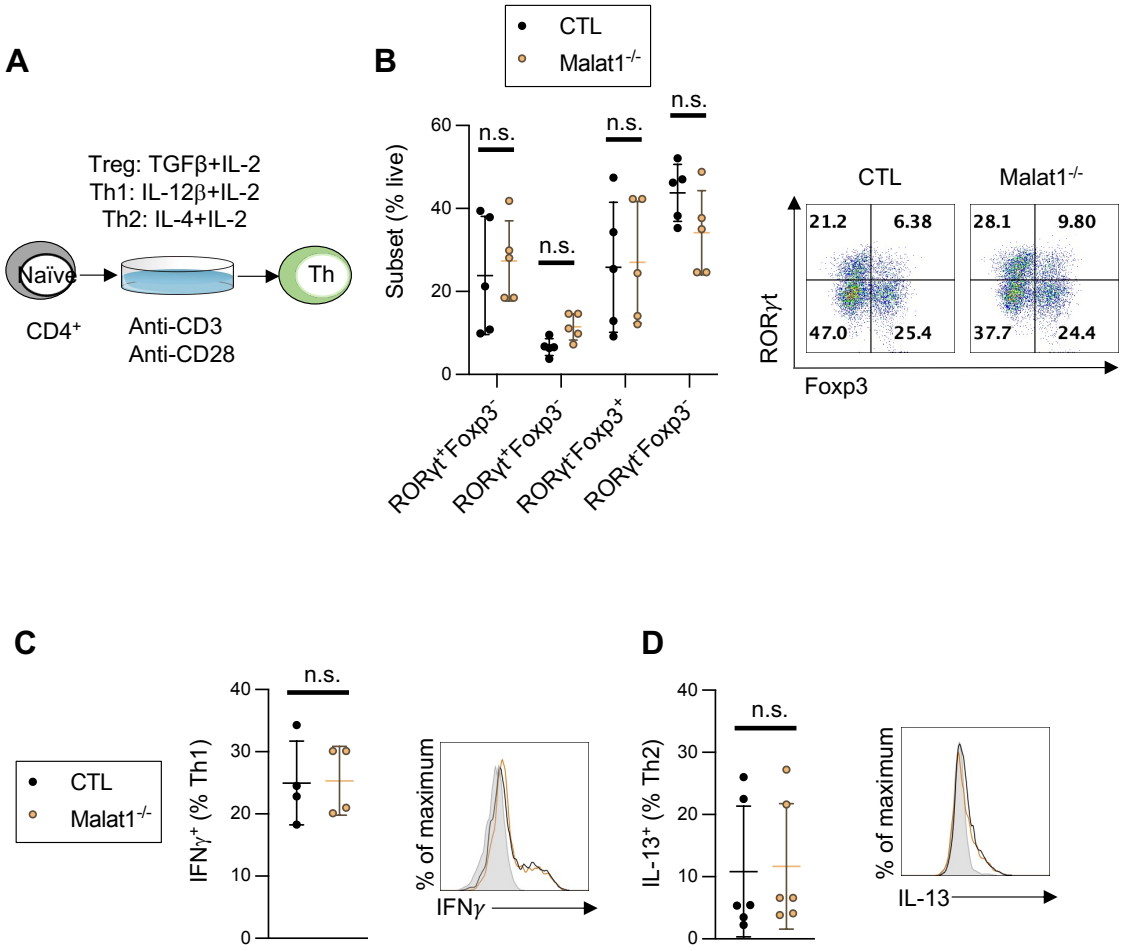

Figure S3. **Malat1 does not regulate Th1, Th2, and Treg generation and function *in vitro*.**

A. Workflow for polarizing naïve $CD4^+$ T cell toward different T cell subsets *in vitro*.
B. Summarized proportion (left) and representative flow cytometry analysis (right) of RORγt and/or Foxp3 expressing T cells from CTL and $Malat1^{-/-}$ littermates cultured in the presence of TGFβ and IL-2. Each dot represents result from one independent culture. n.s. not significant (paired t-test, n=5).
C. Summarized proportion (left) and histogram (right) of IFNγ expression in cultured Th1 cells from CTL and $Malat1^{-/-}$ littermates. n.s. not significant (paired t-test, n=4).
D. Summarized proportion (left) and histogram (right) of IL-13 expression in cultured Th2 cells from CTL and $Malat1^{-/-}$ littermates. n.s. not significant (paired t-test, n=6).

Figure S4. **Malat1-dependent gene programs in cultured Th17 cells**

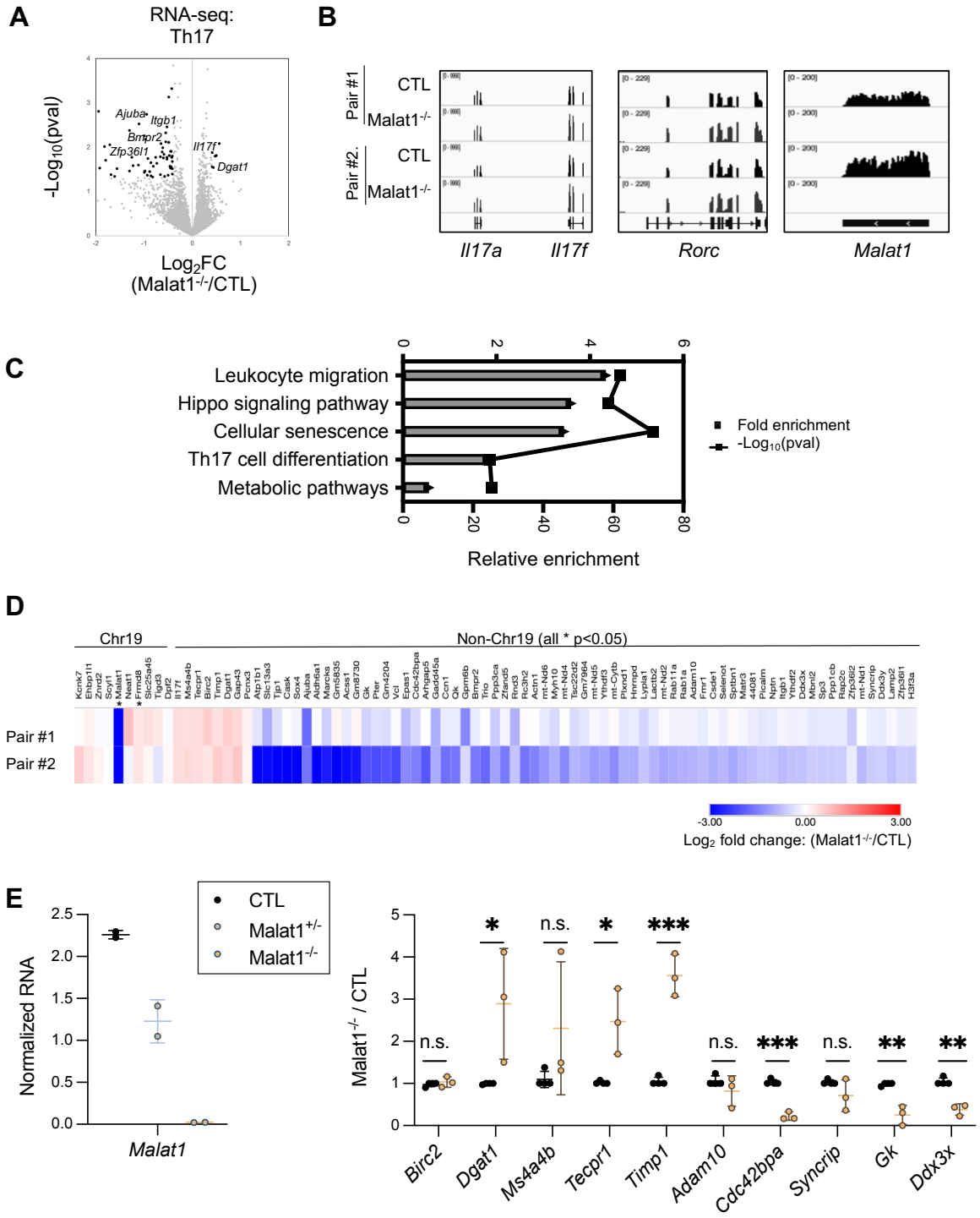

Figure S4. **Malat1-dependent gene programs in cultured Th17 cells.**

A. Volcano plot depicting differential gene expression in Malat1$^{-/-}$ and CTL Th17 cells generated in the presence of anti-CD3, anti-CD28, IL-6, and TGFβ for 3 days from two independent experiments. Black dots: genes with a $\log_2$ fold-change > 0.4 or < -0.4, p-value < 0.05 and minimal counts of 100 (DEseq2) are highlighted in black.
B. IGV browser displaying RNA-seq reads mapping to the *Il17a-Il17f* and *Malat1* locus in cultured Th17 cells from two pairs CTL and Malat1$^{-/-}$ mice.
C. Top KEGG pathways enriched with Malat1-dependent genes in Th17 cells from A.
D. Heatmap displaying average $\log_2$ fold change of *Malat1* neighboring genes (chr19) and Malat1 dependent genes outside of chr19 in cultured CTL and Malat1$^{-/-}$ Th17 cells.
E. Left: Normalized RNA expression of *Malat1* in cultured Th17 cells in Malat1$^{+/+}$, Malat1$^{+/-}$, and Malat1$^{-/-}$ mice. Right: Normalized mRNA expression of the indicated genes in cultured Th17 cells from CTL (Malat1$^{+/+}$ or Malat1$^{+/-}$) and Malat1$^{-/-}$ mice as detected by qRT-PCR. * p-value<0.05, ** p-value<0.01, *** p-value<0.001, n.s. not significant (paired t-test, n=5).

Figure S5. **GRID-seq identified chromatin occupancy of lncRNAs in Th17 cells**

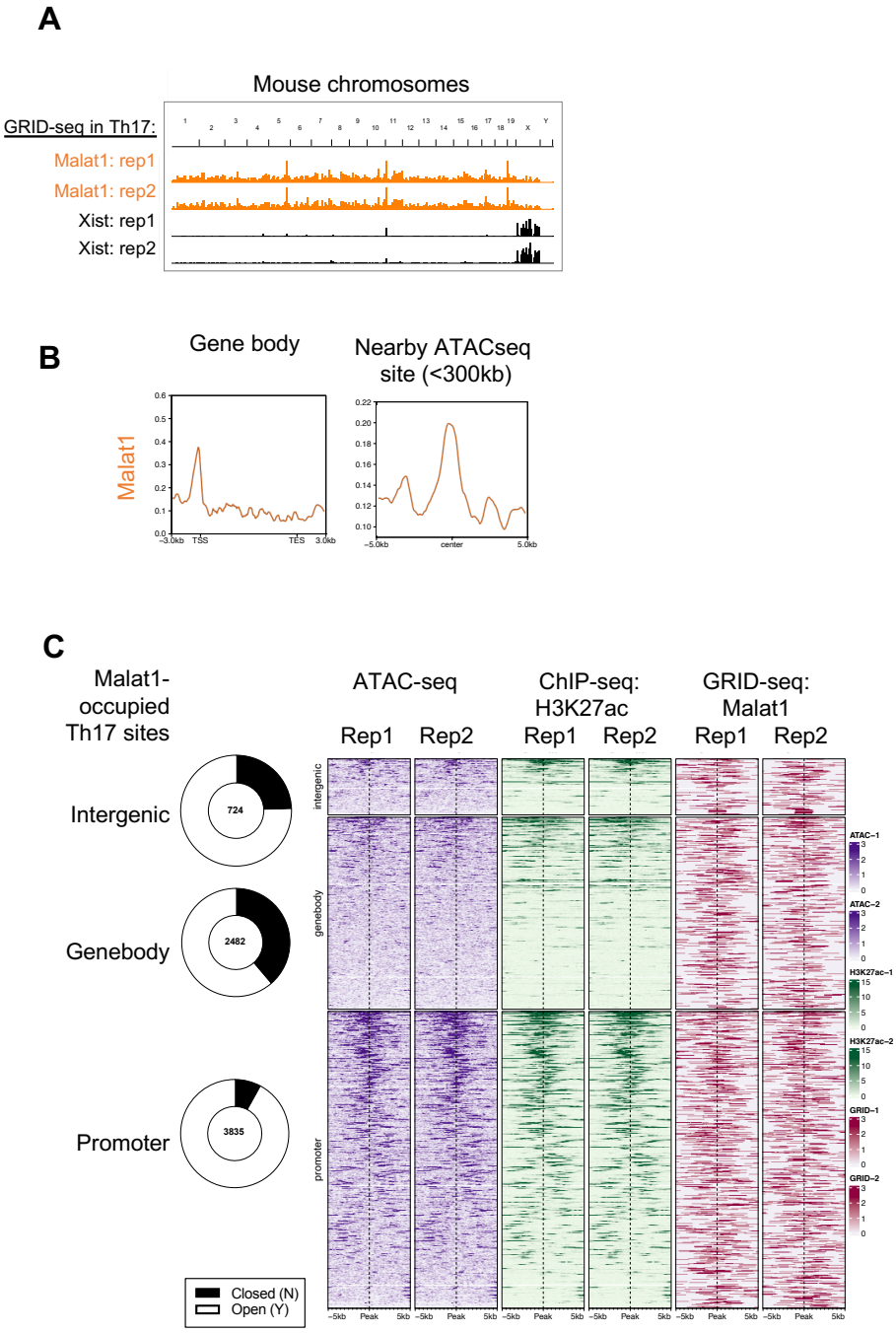

Figure S5. **GRID-seq identified chromatin occupancy of lncRNAs in Th17 cells**

A. GRID-seq signals of Malat1 and Xist displaying their genome-wide occupancy on the chromatin in two biological replicates of Th17 cells.
B. Left: Malat1 chromatin occupancy on the gene body of Malat1 targets (defined as those with >-0.4 log2 fold change in Malat1$^{-/-}$ Th17 cells compared to control). Right: Malat1 chromatin occupancy in a 5kb window around the putative enhancers of Malat1 targets (defined as those with >-0.4 log2 fold change in Malat1$^{-/-}$ Th17 cells compared to control).
C. Open chromatin (ATAC-seq), H3K27ac (ChIP-seq), and Malat1 (GRID-seq) signals on Malat1 occupying peaks. Th17 promoters (3,834 total) were defined as 2.5kb genomic regions flanking TSS; DREs (2,476 total) were defined as those within 12.5kb of a H3K27ac peak; gene bodies (6,166 total) were scaled displayed of first TSS to the last TTS of each annotated gene.

Figure S6. **Malat1 chromatin occupancy on selected direct target genes in Th17 cells**

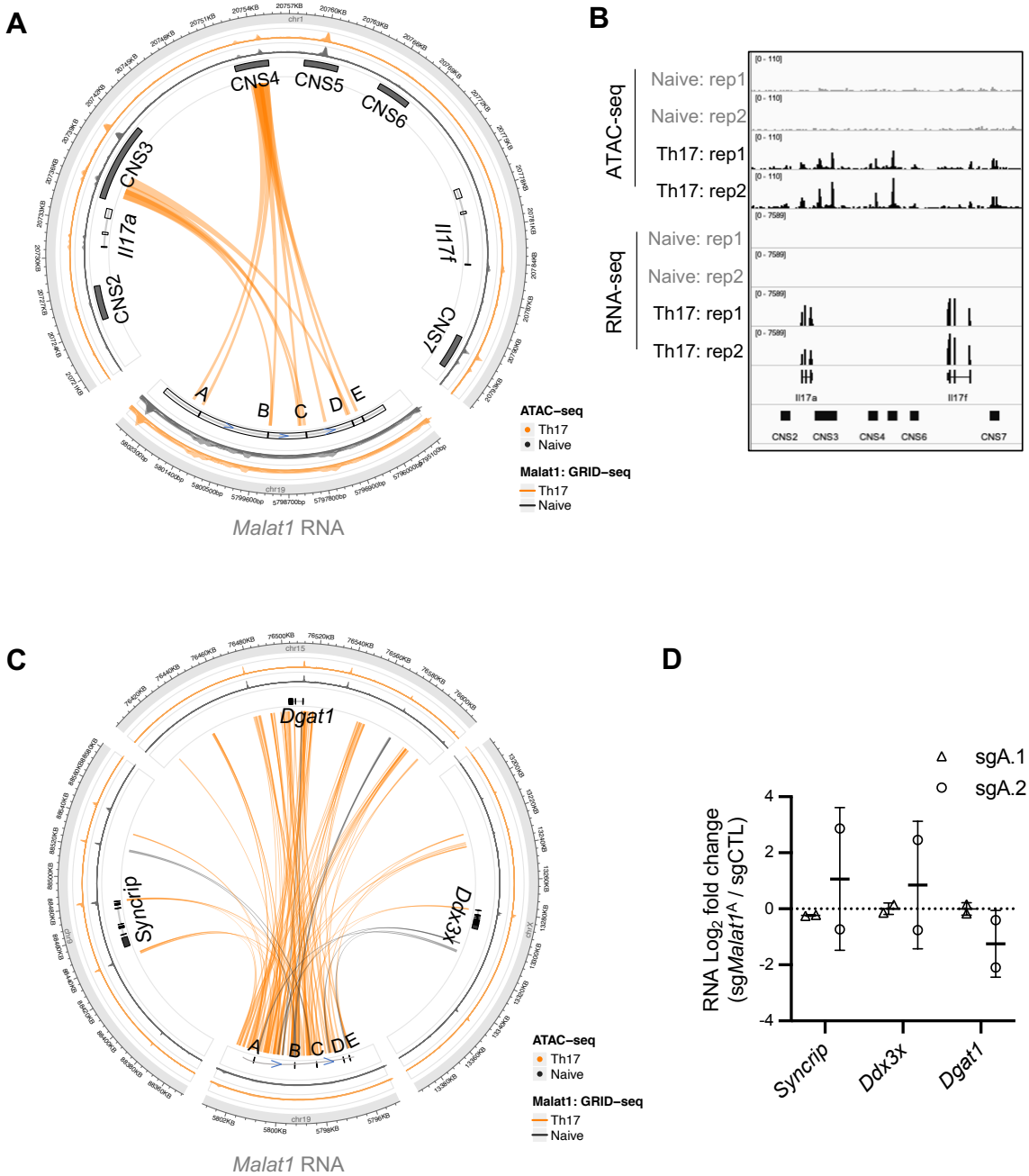

Figure S6. **Malat1 chromatin occupancy on selected direct target genes in Th17 cells**

A. Circos plot showing Malat1 trans-interactions (Th17: orange lines, Naïve: grey line) detected by GRID-seq at the *Il17a-Il17f* locus in CTL Th17 cells. Five Malat1 RNA regions enriched on the *Il17a-Il17f* locus were designated as A-E. The outer circles show signals of ATAC-seq (dark grey, averaged signals from two independent replicate), H3K27ac (ChIP-seq, red, averaged signals from two independent replicate), and p300 (ChIP-seq from GSE40918 (*85*), blue).
B. IGV browser of ATAC-seq and RNA-seq results from two independent replicates of naïve and Th17 cells at the *Il17a-Il17f* locus.
C. Circos plot showing interactions (Th17: orange lines) between Malat1 RNA and genomic DNA at the indicated loci in CTL Th17 cells detected by GRID-seq. The outer circles show signals from ATAC-seq (dark grey) and H3K27ac (ChIP-seq, red).
D. Summarized $\log_2$ fold change of mRNA ratio of indicated genes in cultured Th17 cells from CTL or Malat1$^{-/-}$ mice. * p-value<0.05 (paired t-test, n=2).